

Review

# Rational Design of the Catalysts for the Direct Conversion of Methane to Methanol Based on a Descriptor Approach

Zhi Li <sup>1</sup>, Yanjun Chen <sup>1</sup>, Zean Xie <sup>2</sup>, Weiyu Song <sup>1,\*</sup>, Baijun Liu <sup>1,\*</sup> and Zhen Zhao <sup>1,2,\*</sup>

<sup>1</sup> State Key Laboratory of Heavy Oil Processing, China University of Petroleum, Beijing 102249, China; lizhi817@126.com (Z.L.); yanjunchen2018@163.com (Y.C.)

<sup>2</sup> Institute of Catalysis for Energy and Environment, Shenyang Normal University, Shenyang 110034, China; xiezean@126.com

\* Correspondence: songwy@cup.edu.cn (W.S.); bjliu@cup.edu.cn (B.L.); zhenzhao@cup.edu.cn (Z.Z.)

**Abstract:** The direct oxidation of methane to methanol as a liquid fuel and chemical feedstock is arguably the most desirable methane conversion pathway. Currently, constructing and understanding linear scaling relationships between the fundamental physical or chemical properties of catalysts and their catalytic performance to explore suitable descriptors is crucial for theoretical research on the direct conversion of methane to methanol. In this review, we summarize the energy, electronic, and structural descriptors used to predict catalytic activity. Fundamentally, these descriptors describe the redox properties of active sites from different dimensions. We further explain the moderate principle of descriptors in methane-to-methanol catalyst design and provide related application work. Simultaneously, the underlying activity limitation of methane activation and active species generation is revealed. Based on the selectivity descriptor, the inverse scaling relationship limitation between methane conversion and methanol selectivity is quantitatively understood. Finally, multiscale strategies are proposed to break the limitation and achieve the simultaneous enhancement of activity and selectivity. This descriptor-based review provides theoretical insights and guidance to accelerate the understanding, optimization, and design of efficient catalysts for direct methane-to-methanol conversion.

**Keywords:** methane activation; direct oxidation to methanol; scaling relationship; descriptor; conversion–selectivity limit



**Citation:** Li, Z.; Chen, Y.; Xie, Z.; Song, W.; Liu, B.; Zhao, Z. Rational Design of the Catalysts for the Direct Conversion of Methane to Methanol Based on a Descriptor Approach. *Catalysts* **2023**, *13*, 1226. <https://doi.org/10.3390/catal13081226>

Academic Editors: Hongxing Dai and Junhu Wang

Received: 16 July 2023

Revised: 13 August 2023

Accepted: 15 August 2023

Published: 21 August 2023



**Copyright:** © 2023 by the authors. Licensee MDPI, Basel, Switzerland. This article is an open access article distributed under the terms and conditions of the Creative Commons Attribution (CC BY) license (<https://creativecommons.org/licenses/by/4.0/>).

## 1. Introduction

Methane, with its large reserves and relatively low cost when obtained from natural gas, coalbed methane, and shale gas, is arguably the most promising feedstock [1]. However, most natural gas fields are located in remote regions, and some of the natural gas can only be flared due to its low economic value, resulting in resource waste and environmental pollution [2]. Direct methane-to-methanol conversion is the ideal way to significantly reduce transportation and storage costs [3]. Methane is thermodynamically highly stable and not easily activated, whereas methanol, with a lower C–H bond strength compared to methane, is more susceptible to deep oxidation to CO<sub>2</sub> with the same active sites [4]. Therefore, efficient methane activation while ensuring methanol selectivity is one of the biggest challenges in the field of energy research [5].

Extensive efforts have been made to explore new catalytic systems and design strategies for direct methanol production from methane under mild conditions with controlled oxidation processes [6–8]. In particular, enzyme-mimetic single-site catalysts, with the advantages of both heterogeneous and homogeneous catalysts, have excellent potential in direct methane-to-methanol conversion [9]. Therefore, many enzyme-mimetic single-site heterogeneous catalysts with different support types have been prepared, such as metal-exchanged zeolites [10], metal-organic frameworks (MOFs) [11], two-dimensional (2D)

nanomaterials [12], and others [13–15]. Increasing numbers of pioneering catalytic design strategies with various combinations [16,17] of active site configurations, coordination environments, and topological features have been proposed and validated. However, due to the limitations arising from operando characterization techniques and the simultaneous presence of various species under operating conditions, many relevant reaction mechanisms have yet to be revealed [18].

Computational modeling has provided us with a powerful tool, especially in active site identification, intermediate species determination, and reaction path construction [19]. Currently, one of the crucial goals in computational catalysis is to establish and understand structure–activity relationships between the fundamental properties of catalytic materials and their catalytic performance [20], as this understanding will lay the theoretical foundation for achieving a more efficient and rational design of catalysts [21]. Therefore, establishing linear scaling relationships between catalytic performance (e.g., activity, selectivity, and stability) and the physical or chemical properties of the catalytic system (e.g., energy changes, geometric structures, and electronic structures) as descriptors is crucial [22].

Recently, significant advances have been made in descriptor-based theoretical work on catalyst design for different reactions [23–25]. Based on suitable descriptors, complex and high-dimensional variables in catalytic systems can be reduced to simplify the research models [26,27], and catalyst optimization will be a more targeted process [28]. Subsequently, the screening process and screening window [29] based on the scaling relationships and descriptors can be established in order to quickly and accurately predict catalytic performance, achieving the efficient screening of high-throughput catalysts [30]. At the same time, we can quantitatively identify and understand the optimization laws and limitations [31] of different regulation methods in catalyst design. Moreover, reasonable strategies to break the limitations can be proposed to further improve catalytic performance [32].

Therefore, the present review focuses on the direct methane-to-methanol reaction to summarize the progress of descriptor-based catalyst design. First, the energy, electronic, and structural descriptors are summarized to predict catalytic activity. We further explain the intrinsic correlation, the moderate principle, and the underlying limitations of activity descriptors in methane-to-methanol catalyst design, and we provide related application work. Furthermore, based on the selectivity descriptor, we can understand and provide strategies to break the conversion–selectivity limit. Finally, based on pioneering multiscale design work, we propose strategies combining multiple variables to break the existing bottlenecks in order to achieve simultaneous improvement in the activity and selectivity of direct methane-to-methanol conversion.

## 2. Methane Activation Mechanisms

The C–H bond breakage of methane is the critical step in direct methane-to-methanol conversion. In heterogeneous systems, reaction mechanisms for methane activation with the C–H bond breakage in methane are mainly divided into homolytic and heterolytic mechanisms [33,34] with the different properties of active sites and reaction pathways, as seen in Figure 1.

### 2.1. Homolytic Mechanisms

Homolytic mechanisms involve hydrogen atom abstraction from CH<sub>4</sub> via active oxygen species in M–O active sites to form a free methyl radical and a hydrogen atom adsorbed on the catalyst surface [35] with three-center linear transition states. In its final state, the generated methyl radical has sp<sup>2</sup> hybridization and a trigonal planar geometry [36]. It cannot form M–C bonds with active sites and has weak interactions with OH groups. Meanwhile, a one-electron redox process occurs, leading to the oxidation of the carbon center from the –4 state to the –3 state and the corresponding reduction of the active sites. The homolytic mechanisms generally require strong oxidizing oxidants (e.g., H<sub>2</sub>O<sub>2</sub> and N<sub>2</sub>O) [37,38] and high metal oxidation states to form electron-deficient

species (e.g.,  $O^-$  and  $O^{2-}$ ) [39,40], resulting in promotion of the homolytic dissociation of C–H bonds.

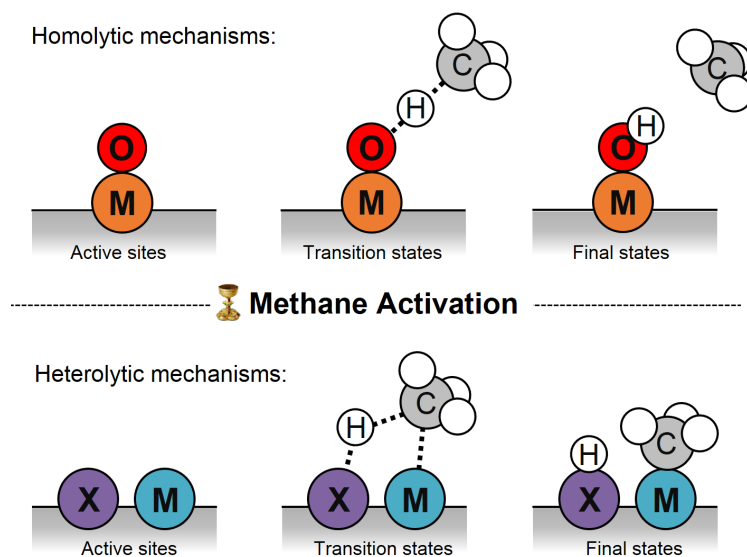


**Figure 1.** Comparison of active sites and reaction pathways in methane activation via homolytic and heterolytic mechanisms.

## 2.2. Heterolytic Mechanisms

Heterolytic mechanisms generally use surface Lewis acid–base pairs (M–X) as active sites to dissociate the adsorbed methane to produce  $CH_3^-$  and  $H^+$  with four-center quadrilateral transition states [34,41]. In the final state, the M metal atom stabilizes the  $sp^3$ -hybridized methyl group in a tetrahedral geometry via the  $\sigma$ -bond [42]. At the same time, hydrogen protons are accepted through the X atom, including surface nucleophilic oxygen species, surface metals, and ligands. Thus, the heterolytic mechanism is also called the surface-stabilized mechanism [43]. Unlike homolytic mechanisms, the carbon and active centers maintain unchanged oxidation states in heterolytic mechanisms [44]. Furthermore, the M–O active site, with a low metal oxidation state in the heterolytic mechanism, is more favorable for the formation of electron-saturated oxygen atoms ( $O^{2-}$ ) [27,45] to accept hydrogen protons and promote the heterolytic dissociation of C–H bonds. However, although the two mechanisms have different characteristics, the accurate judgment of the methane activation mechanism by various active sites still requires a comparison of transition state energies [43].

In addition to homolytic and heterolytic mechanisms, several methane activation processes can proceed through free radicals such as  $\bullet OH$  [46]. However, the C–H bond breakage process in these systems often occurs in the liquid phase or in gas environments with free radicals, and the reaction performance is mainly determined by the concentration of free radicals generated on the catalyst. Meanwhile, there is no direct interaction between methane with the active species on the catalyst. Therefore, this methane activation mechanism will not be included in this review.

## 3. Activity Descriptors

Currently, no catalysts have been found for the direct conversion of methane to methanol in industrial production [5,47]. This reaction process without deep oxidation is extremely difficult due to kinetic and thermodynamic limitations [48]. C–H bond breakage is the first prerequisite and challenge for direct methane conversion [49]. Thus, developing activity descriptors with accessible properties of catalytic systems to understand the activity of active sites is critical; these descriptors are based on scaling relationships [50,51]. With suitable activity descriptors, we can directly judge whether catalysts have the capacity to

activate methane and should be examined further by experimental and complete reaction path calculations [52,53].

### 3.1. Activity Descriptors for Homolytic Mechanisms

The catalysts used via homolytic mechanisms mainly include zeolites, MOFs, and 2D materials, and have a similar methane active site (M–O), transition state (three-center linear transition states), and final state (M–OH +  $\bullet$ CH<sub>3</sub>). Therefore, in addition to the traditional Bronsted–Evans–Polanyi (BEP) relationship [54], Latimer and co-workers [55] demonstrated that hydrogen affinity energy ( $E_H$ ), which is defined as the energy difference between M–OH and M–O in active sites, is a universal descriptor that can be used to predict methane activation barriers ( $E_{TS}$ ) via homolytic mechanisms (Figure 2a). The linear scaling relationship between  $E_{TS}$  and  $E_H$  indicates that active sites of methane activation with a lower  $E_H$  (i.e., a stronger O–H bond) will have more stable transition states to reduce  $E_{TS}$ .

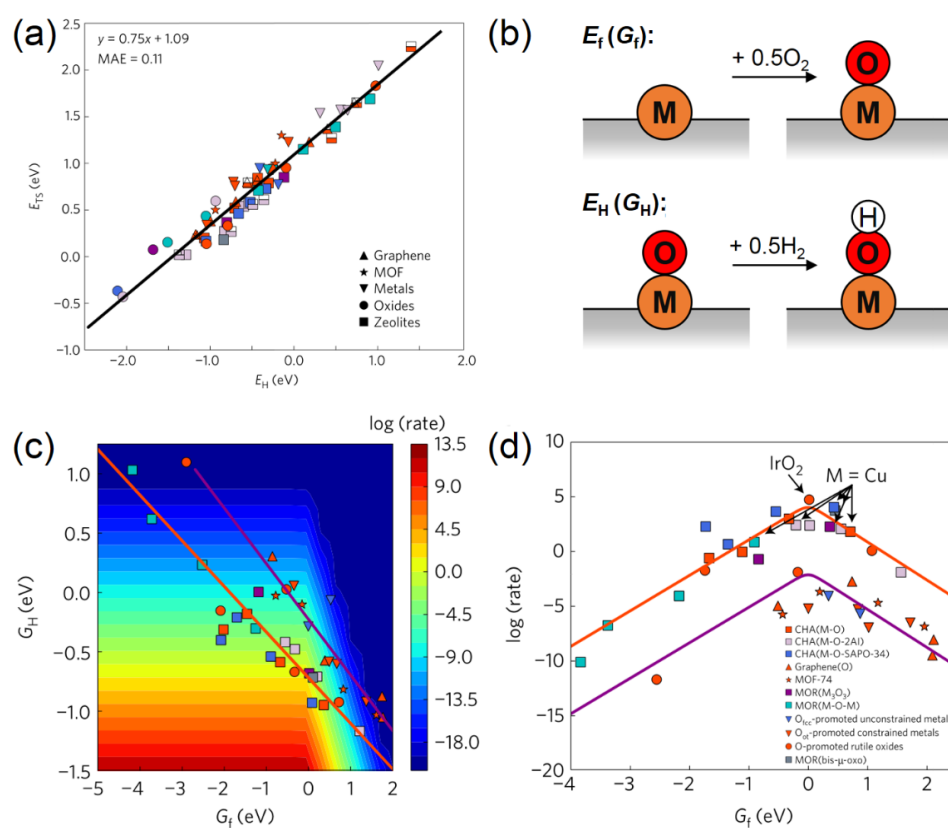


**Figure 2.** (a) Linear scaling relationships between  $E_{TS}$  and  $E_H$  via homolytic mechanisms. (b) Schemes representing  $E_f(G_f)$  and  $E_H(G_H)$ . (c) Two-dimensional rate plots with  $G_H$  and  $G_f$  as descriptors. (d) One-dimensional volcano rate curves using  $G_f$  as a descriptor. Reprinted/adapted with permission from Ref. [55]. Copyright 2016, copyright Springer Nature Limited.

Furthermore, the methane activation rate is only related to  $G_f$  (active site formation energy which is the free energy of the oxidation process of reduced active sites, describing the fraction of available active sites) and  $G_H$  (describing the capacity of methane activation) under specific temperature and pressure conditions. Meanwhile,  $G_f$  is linearly negatively correlated with  $G_H$  in two scaling lines (Figure 2c). The physical origin of these two lines is due to the different charge delocalization abilities of substrates during the formation of the active site. Therefore, a  $G_f$ -related volcano curve can be constructed to predict the methane activation rate (Figure 2d). To reach the highest theoretical rate (i.e., the top of the volcano curve),  $G_f$  should be approximately 0 eV to achieve the optimal balance between active site coverage and methane activation ability. The volcano curve indicates that Cu-exchanged zeolites and IrO<sub>2</sub> are close to the summit of the volcano curve, and some of these catalysts

have been experimentally proven to have excellent methane activation properties [42,56,57]. Therefore, the rationality of this volcanic relationship has been confirmed, which can serve as an initial guide in methane conversion catalyst discovery with homolytic mechanisms. Moreover, as shown in Figure 3, the oxygen vacancy formation energy ( $\Delta E_{\text{vac}}$ ) [58] is also considered a predictor to evaluate methane activation energies in various oxide-based catalysts, including doped MgO, doped CeO<sub>2</sub>, doped TiO<sub>2</sub>, TbO<sub>x</sub> with different oxidation states, and TiO<sub>2</sub> with various surface facets. It indicates that the more easily surfaces are reduced (i.e., a lower  $\Delta E_{\text{vac}}$ ), the stronger the catalyst's ability to activate methane (i.e., a lower  $\Delta E_{\text{act}}$ ).

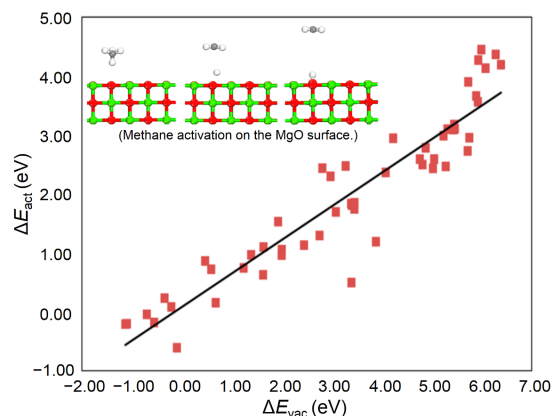


**Figure 3.** Linear scaling relationships between methane activation energies ( $\Delta E_{\text{act}}$ ) and oxygen vacancy formation energies ( $\Delta E_{\text{vac}}$ ) in various oxide-based catalysts (red squares), including doped MgO, doped CeO<sub>2</sub>, doped TiO<sub>2</sub>, TbO<sub>x</sub> with different oxidation states, and TiO<sub>2</sub> with various surface facets. Reprinted/adapted with permission from Ref. [58]. Copyright 2016, copyright American Chemical Society.

### 3.2. Activity Descriptors for Heterolytic Mechanisms

For most metal and metal oxide catalysts, unsaturated coordination metal sites can stabilize methyl groups during methane activation via heterolytic mechanisms. Recently, a generalized linear relationship was proposed by Latimer et al. [43] to evaluate the  $E_{\text{TS}}$  of methane heterolytic dissociation in terms of the final-state energy ( $E_{\text{FS}}$ ), which is determined by the sum bond energies of H<sup>+</sup> and CH<sub>3</sub><sup>−</sup> on the surface (Figure 4a). This linear relationship is the result of the similar methane active site (M–X), transition state (four-center transition states), and final state (M–CH<sub>3</sub> + X–H). In the activation of methane via heterolytic mechanisms, an active site with a lower EFS is more capable of stabilizing the transition state with a lower  $E_{\text{TS}}$ .

However, methane activation mechanisms (heterolytic or homolytic mechanisms) in different catalysts must be correctly evaluated in advance to select the corresponding suitable descriptor ( $E_{\text{H}}$  or  $E_{\text{FS}}$ ) to calculate the transition energy ( $E_{\text{TS}}$ ). Thus, a simple model has been formulated to predict the methane activation energy (Figure 4b) in a given catalyst site. Using  $E_{\text{TS}}$  calculated from the previously described universal homolytic ( $E_{\text{H}}$ ) and heterolytic ( $E_{\text{FS}}$ ) descriptors, the lower of the two calculated results represents the more accurate  $E_{\text{TS}}$ . By the applicability of this model, we can achieve rapid judgment and prediction of the methane activation mechanisms with the energy barriers, and evaluate many different materials to discover more efficient catalysts. Furthermore, Fung et al. demonstrated that the methane absorption energy ( $E_{\text{ads}}$ ) [59] can be used as the descriptor to measure the low-temperature activity of methane heterolysis on M<sub>1</sub>-TiO<sub>2</sub>(110). The stronger absorption of methane as a pre-activation state proves the enhanced charge and orbital interactions of methane on TiO<sub>2</sub> surfaces, facilitating methane heterolysis via the lower activation energy. Computational studies predict that M<sub>1</sub>-TiO<sub>2</sub>(110) with Rh, Pd, Os, Pt, and Ir atoms will realize low-temperature (<25 °C) methane activation.

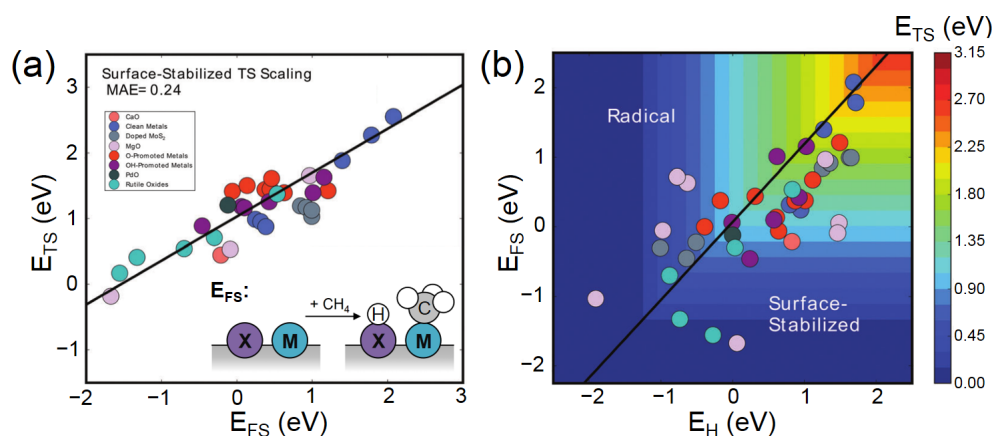


**Figure 4.** (a) Scaling relationships between  $E_{TS}$  and  $E_{FS}$  in heterolytic mechanisms (surface-stabilized mechanisms). The inset shows the schematic representation of  $E_{FS}$  in the methane heterolytic activation. (b) Models for predicting  $E_{TS}$  with  $E_H$  and  $E_{FS}$ . The black line indicates two descriptors predicting equal  $E_{TS}$ . Reprinted with permission from Ref. [43]. Copyright 2017, copyright Royal Society of Chemistry.

### 3.3. Additional Electronic and Structural Descriptors

Furthermore, although the above-mentioned energy descriptors via the adsorption strength of different adsorbates can be used to depict the methane activation properties of various active sites, it is crucial to identify the intrinsic properties of active sites or components that contribute to these binding energies [60] in order to directly predict the activity of methane conversion catalysts without computing additional energies.

For electronic descriptors, the spin density ( $\rho_O$ ) of absorbed oxygen species has been proposed as a common property influencing methane activation [61,62]. A higher spin density indicates that the active oxygen species has more obvious free-radical characteristics and thus a stronger ability to bind the hydrogen atom of methane with a lower activation energy. Meanwhile, the M–O bond order can also be directly related to the stability of active oxygen species ( $E_f$ ) in various MOFs [63]. A lower M–O bond order corresponds to a higher  $E_f$  and a lower methane activation energy. Moreover, Filonowich et al. [64] reported that the charge of the active metal center, as an electronic activity descriptor, can predict methane-to-methanol performance in phthalocyanine-/porphyrin-functionalized graphene (GMPc/GMP) materials with different metal centers, doping substrates, and ligands. As shown in Figure 5, as the charge of the metal center decreases, the methane activation energy decreases linearly, and the oxygen species generation energy increases linearly. As a result, GCoPc series catalysts represent an optimal candidate in direct methane-to-methanol reactions.

Ideally, a more fundamental and straightforward descriptor is desired for activity prediction on the basis of the element-related properties, requiring no additional calculation costs [19,22]. Surprisingly, Zha et al. [65] demonstrated that the ionization energy of active metal atoms as a descriptor is linearly proportional to the adsorption energy of absorbed intermediates over many materials, including zeolites, graphene, transition metal oxides, and single-site alloys. This descriptor is an intrinsic chemistry property of the specific metal element, where a higher ionization energy will lead to a lower  $d$  band and filling more electrons in the antibonding state, resulting in the lower adsorption energy of the intermediates. The descriptor was successfully applied to direct methane-to-methanol conversion. As displayed in Figure 6, with the increase in the second ionization energy, the generation energy of M–O–M active sites linearly increases, whereas the formation energies of other intermediate species all linearly decrease, describing the critical stages of the complete conversion of methane to methanol. Meanwhile, other examples in this work reveal the potential of ionization energies with applications in other surface reactions.

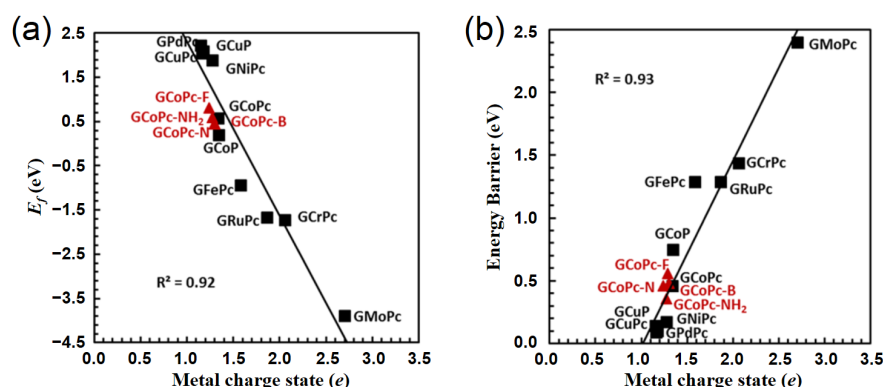


**Figure 5.** Linear scaling relationships between the metal charge state and (a) the active oxygen species formation energy ( $E_f$ ) and (b) the methane activation energy barrier. Black squares represent the GMPc and GMP systems. Red triangles represent the GCoPc system with graphene substrate modified with N and B dopings, and GCoPc with  $\text{NH}_2$  and F ligands. Reprinted/adapted with permission from Ref. [64]. Copyright 2020, copyright American Chemical Society.

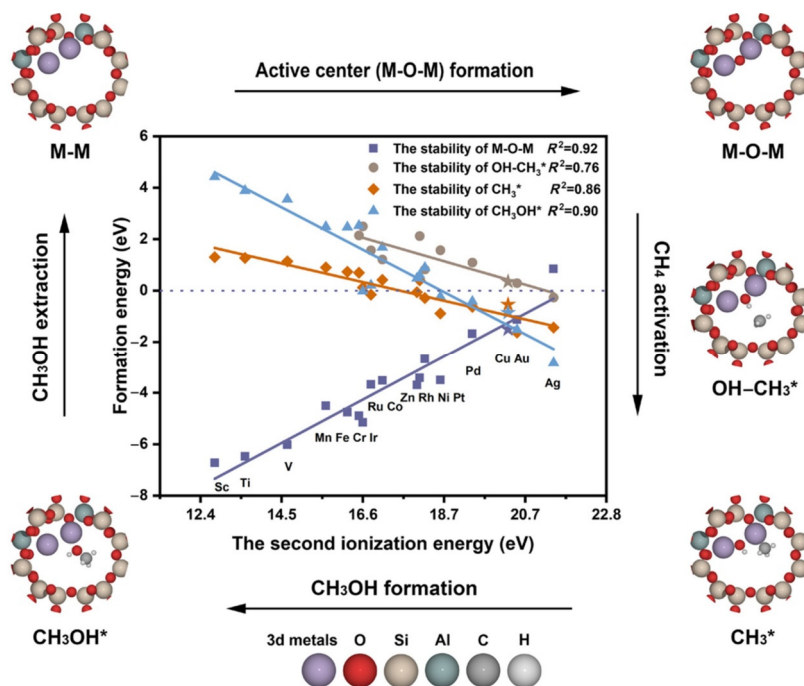


**Figure 6.** Linear scaling relationships between the formation energies of M-O-M,  $\text{OH-CH}_3^*$ ,  $\text{CH}_3^*$ , and  $\text{CH}_3\text{OH}^*$  intermediate species and the second ionization energy descriptor. Reprinted/adapted with permission from Ref. [65]. Copyright 2020, copyright Chinese Chemical Society.

In addition to the above-mentioned electronic descriptors, structural descriptors [66] have been used to predict catalytic performance using geometric structures, which allows us to construct specific active site configurations to design methane conversion catalysts. For example, the stability of active oxygen species ( $E_f$ ) is inversely scaled to the M–O bond length for methane activation in various MOFs: a larger M–O bond length corresponds to a higher  $E_f$  and a lower activation energy, as suggested by Rosen et al. [63]. In Cu-based zeolites with  $[\text{Cu}_2(\mu\text{-O})]^{2+}$  sites for direct methane-to-methanol conversion, as displayed in Figure 7a, Mahyuddin et al. [67] demonstrated that a smaller Cu–O–Cu angle leads to a lower acceptor orbital energy in the active site to stabilize the transition state and reduce the methane activation energy, ultimately leading to diverse catalytic properties. Furthermore, Fung and co-workers [68] defined the adjusted coordination number (ACN), which shows great potential in directly predicting methane activation energies by combining different

coordination numbers of active oxygen atoms and surrounding metal atoms on the surface of metal oxides. As displayed in Figure 7b, the linear scaling relationship indicates that active sites with a small ACN value can more efficiently activate methane with lower energy barriers.

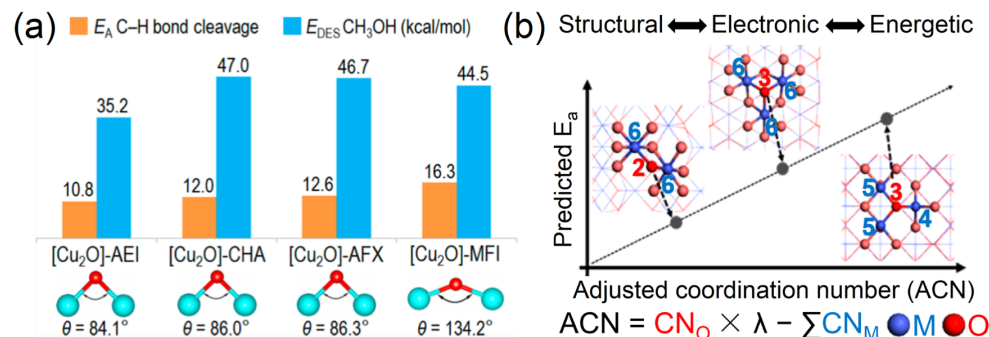


**Figure 7.** (a) Influence of the Cu–O–Cu angle in different zeolites for direct methane-to-methanol conversion. Reprinted/adapted with permission from Ref. [67]. Copyright 2017, copyright American Chemical Society. (b) Linear scaling relationships between the methane activation energy with the ACN descriptor. Red and blue numbers represent coordination numbers of reactive oxygen atoms ( $CN_O$ ) and neighboring metal atoms ( $CN_M$ ), respectively. Reprinted/adapted with permission from Ref. [68]. Copyright 2017, copyright American Chemical Society.

### 3.4. Moderate Principles Based Descriptors in Catalyst Design

Fundamentally, as depicted in Figure 8a, in the methane-to-methanol reaction cycle, active site formation is an oxidation process, and methane activation is a reduction process for active centers, resulting in the descriptors of the two processes (e.g.,  $E_f$  and  $E_H$ ) being negatively correlated [63]. Meanwhile, the intrinsic redox properties of active sites ultimately determine the relative abilities of the oxidation and reduction processes to change the adsorption energies of intermediates in the chemical reaction, resulting in different catalytic properties. Therefore, essentially, the above-mentioned energy, electronic, and structural descriptors all describe the ability of active sites to gain and lose electrons (i.e., the redox property) during the redox process from different dimensions, resulting in a certain scaling correlation with each other [63]. For example, the  $d$ -band center, which is the earliest and most widely used descriptor, uses the  $d$ -band [69–71] to largely describe the variations in the intrinsic redox properties in active sites. With a higher  $d$ -band center, the antibonding state will be elevated and filled with fewer electrons, resulting in a stronger interaction with O\* adsorbates and an increased reductivity of active sites [22]. Meanwhile, the corresponding oxidizability of active sites will be weakened.

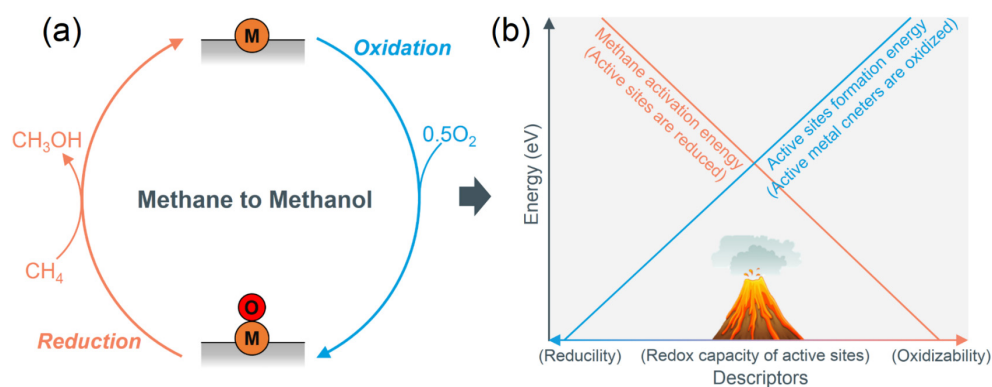


**Figure 8.** Schematic representations in direct methanol production from methane with (a) the whole reaction cycle and (b) linear scaling relationships based on various descriptors in oxidation and reduction processes.

From the perspective of descriptor selection, a simpler descriptor is more convenient for predicting catalytic performance. However, a simpler descriptor contains more limited information, resulting in the linearity of scaling relationships being relatively weak in many catalytic materials. Therefore, for practical applications, accuracy and speed must be balanced according to specific needs and to select the appropriate descriptor for catalyst design [19,29]. At the same time, we must further explore new descriptors, including both electronic and structural properties in catalysts, to evaluate catalytic performance more accurately and quickly.

Furthermore, it is essential to determine the value of descriptors corresponding to the highest catalytic activity (i.e., the screening window). The Sabatier principle [72] will give us a conceptual framework to qualitatively guide catalyst design. When the adsorbed species have a moderate “bond strength”, it is possible to simultaneously achieve effective activation of reactants and rapid desorption of products while avoiding catalyst deactivation, ultimately resulting in a volcano-type relationship between catalytic activity and “bond strength”. At the same time, this moderate principle can also be understood based on the catalytic reaction cycle. When active sites have moderate oxidation and reduction properties that balance the critical elementary steps in the chemical reaction, the overall catalytic activity is the highest [29].

Meanwhile, descriptors based on different dimensions create opportunities to quantitatively characterize the redox properties of active sites, which are the quantitative values to represent the “bond strength” in the Sabatier principle. As shown in Figure 8b, we can determine the range of the screening window corresponding to the optimal-catalyst-based moderate values in different descriptors, where the oxidation process of active species formation is balanced with the reduction process of methane activation [73–75]. For example, we mentioned above the  $G_f$ -related volcano curve for the rate of methane activation (Figure 2d). To design catalysts with the highest theoretical rate of methane conversion based on this model,  $G_f$  should be approximately 0 eV to achieve the optimal balance between active site coverage and methane activation ability. Rosen et al. [63] reported structure–activity relationships in methane activation for a large number of MOFs with different combinations of metal centers and support configurations. As depicted in Figure 9a, the methane activation energy ( $E_{a,C-H}$ ) of various active sites has a negative linear relationship with the active species formation energy ( $\Delta E_O$ , which is the same as the above-mentioned  $E_f$ ). Meanwhile, the active sites of MOFs with later transition metals tend to have a more robust ability to activate methane (i.e., a lower  $E_{a,C-H}$ ) and a lower stability (i.e., a higher  $\Delta E_O$ ). Moreover, the spin density of active oxygen species ( $\rho_O$ ) and the M–O bond distance ( $d_{M-O}$ ) are both considered descriptors of methane activation and active species stability (Figure 9b,c). Meanwhile, the negative scaling relationship between methane conversion and oxygen species stability indicates that the ideal active site needs to have moderate redox properties, and the corresponding screening windows can be determined by different descriptors. Therefore, the M–O active sites in MOFs with the screening window ( $\Delta E_O$ :  $-1\sim 0$  eV,  $\rho_O$ :  $0.4\sim 0.5$ , and  $d_{M-O}$ :  $1.65\sim 1.70$  Å) can satisfy both activity and oxygen species stability requirements. In general, the moderate principle, based on activity descriptors characterizing the redox property in active sites, will provide a robust principle to investigate and initially screen active sites for direct methane-to-methanol conversion.

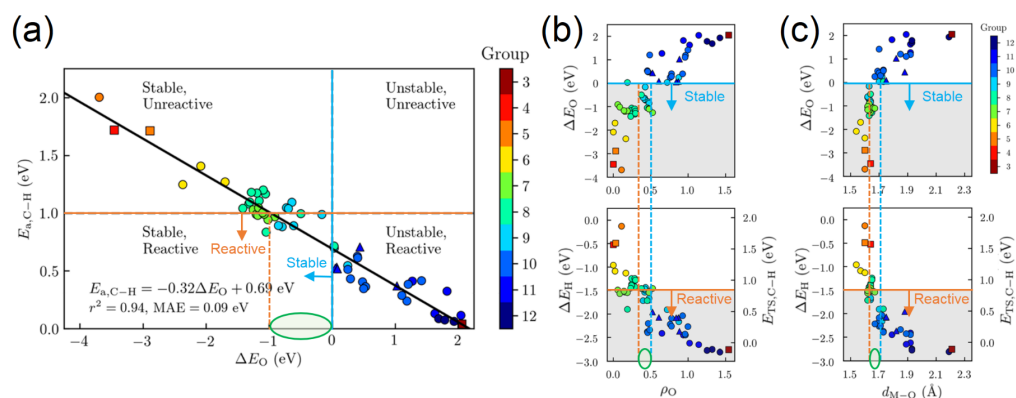


**Figure 9.** (a) Methane activation energies ( $E_{a,C-H}$ ) as functions of  $\Delta E_O$  and the group number of the active metal.  $\Delta E_O$  and  $\Delta E_H$  as functions of (b) the absolute spin density of active oxygen species ( $\rho_O$ ) and (c) the M–O distance ( $d_{M-O}$ ). Symbol shape indicates the formal oxidation state of the metal site prior to oxidation as 1+ (triangles), 2+ (circles), or 3+ (squares). Orange and blue lines represent the boundaries of activity ( $E_{a,C-H} < 1$  eV;  $\Delta E_H < -1.51$  eV) and stability ( $\Delta E_O < 0$  eV), respectively. Green circles on the horizontal coordinate indicate the screening windows based on different descriptors. Reprinted/adapted with permission from Ref. [63]. Copyright 2019, copyright American Chemical Society.

### 3.5. Applications of Activity Descriptors

Recently, activity descriptors have been successfully applied to screen catalysts based on zeolites [76], 2D materials [75], and MOFs [53] for direct methane-to-methanol conversion. In this section, we mainly take 2D materials as examples, which have a rich adjustment space, and use activity descriptors to reveal the effect of different regulation approaches on the activity of direct methanol production from methane and screen optimal active sites.

According to the density function theory (DFT) scaling relationship shown in Figure 10a, a single Fe atom confined in a graphene nanosheet (GN) with an O–MN<sub>4</sub>–O (Mn, Fe, Co, Ni, and Cu) active site is near the summit of the volcano rate curve with the descriptor of active species formation energy ( $G_f$ ) [74]. Experiments also first proved that Fe<sub>1</sub>/GN is an excellent non-precious metal catalyst for the direct conversion of methane to high-value-added C1 oxygenated products at 25 °C. Tan et al. [75] explored the influence of vacancies and nonmetallic doping around the O–FeN<sub>4</sub>–O active sites in graphene on direct methane oxidation performance in terms of  $G_f$ . As displayed in Figure 10c,d, FeN<sub>4</sub>-V<sub>6r</sub> and FeN<sub>4</sub>-V<sub>5r</sub> active sites with C vacancies and nonmetal atom-doped P-O/FeN<sub>4</sub> active sites have a  $G_f$  closer to 0 eV compared to the intact FeN<sub>4</sub> site. Thus, the stability of active oxygen species and the ability of methane activation are more balanced in the new active sites, resulting in the calculated methane activation rate of the three candidate sites being more than 1000 times that of the intact FeN<sub>4</sub> active site. On different 2D materials, Wang et al. [77] comprehensively explored the influence of different coordination types (N or O) of the triple-ligand mononuclear Cu active center in the boron nitride (BN) system on the methanol-to-methanol performance in terms of an active oxygen adsorption energy descriptor ( $\Delta G_{ads}$ , which is the same as the above-mentioned  $G_f$ ). As seen in Figure 10b, Cu<sub>1</sub>/O<sub>1</sub>N<sub>2</sub>-BN has the highest reaction performance due to its moderate oxygen adsorption properties.

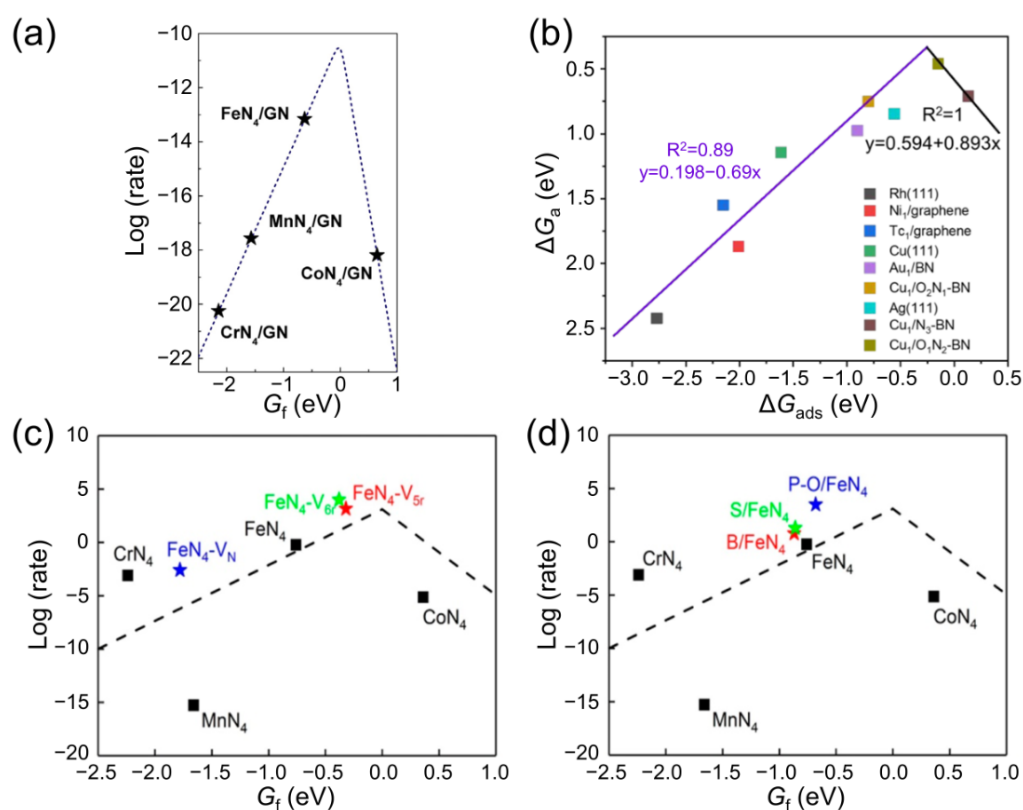


**Figure 10.** Volcano curves of methane activation rate in  $\text{Fe}_1/\text{GN}$  catalysts with (a) intact sites. Reprinted/adapted with permission from Ref. [74]. Copyright 2018, copyright Elsevier Ltd. (b) Volcano curves of rate-limiting step energies in direct methane-to-methanol conversion with the adsorption energy of active oxygen species. Reprinted/adapted with permission from Ref. [77]. Copyright 2022, copyright Royal Society of Chemistry. Volcano curves of methane activation rate in  $\text{Fe}_1/\text{GN}$  catalysts with (c) various vacancies and (d) doping heteroatoms with the descriptor of  $G_f$ . Squares and stars represent intact  $\text{MN}_4$  ( $M = \text{Cr}, \text{Mn}, \text{Fe}, \text{Co}$ ) active sites and defective  $\text{FeN}_4$  active sites, respectively. Reprinted/adapted with permission from Ref. [75]. Copyright 2021, copyright American Chemical Society.

Furthermore, using a descriptor-based approach, we comprehensively investigated the electrochemical methane conversion of 2D carbides (MXenes) [78]. As shown in Figure 11a, using the scaling relationship established by the  $\Delta E_{\text{OH}^*} - \Delta E_{\text{O}^*}$  descriptor in the oxygen evolution reaction (OER) process, most MXenes can form stable oxygen species under a suitable external potential. As shown in Figure 11b, a trade-off relationship between the thermodynamic stability of oxygen species with the reactivity of methane activation ( $\Delta E_{a,\text{TS}}$ ) is established. Based on the  $\Delta E_{\text{OH}^*} - \Delta E_{\text{O}^*}$  descriptor,  $\text{CrHf}_2\text{C}_2\text{O}_2$  and  $\text{TaHf}_2\text{C}_2\text{O}_2$  meet both activity and stability requirements, representing promising catalysts for the electrochemical methane conversion. Furthermore, the  $d$ -band metal center and occupied  $p$ -band oxygen center can be considered to be electronic descriptors due to their scaling relationship with the  $\Delta E_{\text{OH}^*} - \Delta E_{\text{O}^*}$  descriptor (Figure 11c,d). Moreover, MXene selectivity can be flexibly adjusted by applying different potentials. These results give a systematic understanding of the stability, activity, and selectivity of the electrocatalytic methane conversion in MXenes. Therefore, based on reasonable descriptors and the moderate principle, catalytic systems can be designed more efficiently and purposefully to enhance their catalytic performance in direct methane oxidation.



to-methanol conversion also have the potential to negatively or positively deviate from the existing linear relationship when other factors are introduced, including coordination number [63], reversible linker displacement [83], and noncovalent interactions [84]. Overall, attempts to identify events that break the given linear relationship are necessary to better understand and develop methane conversion catalysts with a simultaneously high activity and stability.

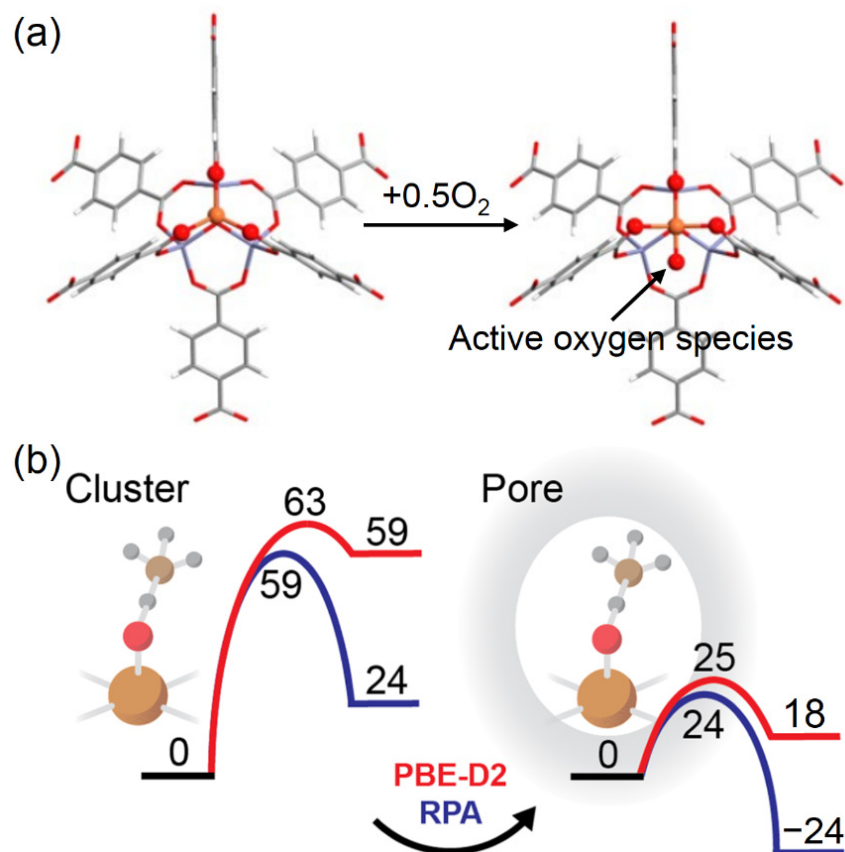


**Figure 12.** (a) Structure change in Fe-MOF-5 with the generation of oxygen active species in the open Fe site. Reprinted/adapted with permission from Ref. [63]. Copyright 2019, copyright American Chemical Society. (b) Comparison of methane activation energies of Fe–O active sites in clusters only and the pore of periodic Fe-SSZ-13 (kJ/mol). Reprinted/adapted with permission from Ref. [82]. Copyright 2016, copyright American Chemical Society.

#### 4. Selectivity Descriptors

##### 4.1. Conversion–Selectivity Limit in Continuous Methane to Methanol

As documented in reports [6], the challenge of direct methane-to-methanol conversion is not only the methane activation but simultaneously maximizing methanol selectivity. From a thermodynamics perspective, with the further oxidation of CH<sub>3</sub>OH to CH<sub>2</sub>O, HCOOH, and CO<sub>2</sub>, the reaction energies are gradually decreasing, as depicted in Figure 13 [85]. Thus, the overoxidation of methanol is thermodynamically more favorable. Meanwhile, methane derivatives with greater polarities and multiple functional groups are highly susceptible to deep oxidation under methane-activation conditions [86]. Based on these considerations, the primary oxygenates (methanol) are prone to further oxidation to CO<sub>2</sub>, resulting in a substantial loss in the selectivity of methanol.

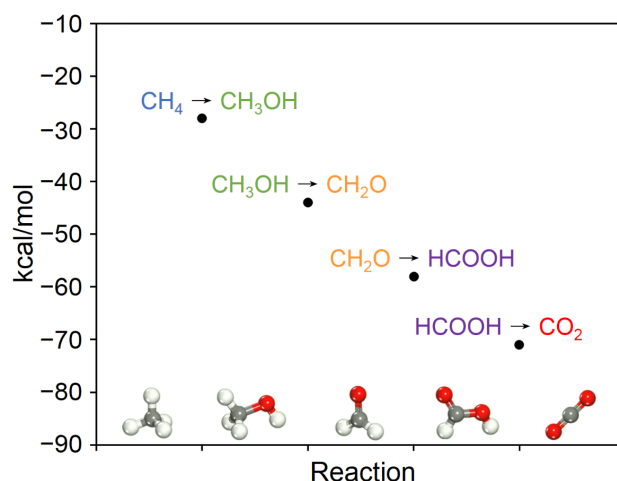


**Figure 13.** Free energies of the continuous oxidation in the  $\text{CH}_4$  to  $\text{CO}_2$  with  $\text{O}_2$  at 298 K. Reprinted/adapted with permission from Ref. [85]. Copyright 2017, copyright American Chemical Society.

Furthermore, Latimer et al. [87] demonstrated a universal trend that the C–H bond activation energy of methane via homolytic mechanisms is 0.40 eV ( $\Delta G^a$ , at 300 K) higher than that of methanol, which exists in many catalytic systems including zeolites, MOFs, metals, and metal oxides. Moreover, a simplified two-step methanol selectivity model ( $\text{CH}_4 \rightarrow \text{CH}_3\text{OH} \rightarrow \text{CO}_2$ ) with  $\Delta G^a$  effectively revealed the conversion–selectivity limit via extensive experimental and DFT data in the direct oxidation of methane to methanol, independent of the choice of catalyst. Therefore, the relationship between methane conversion and methanol selectivity at the specified reaction temperature is only related to  $\Delta G^a$ , which can be used as the methanol selectivity descriptor [48]. These results indicated that direct methanol production from methane via homolytic mechanisms in continuous processes will ultimately be limited in maximizing methane conversion and methanol selectivity simultaneously, where methanol selectivity decreases significantly with increasing methane conversion. As seen in the conversion–selectivity model shown in Figure 14a, when methanol selectivity approaches 100%, the methane conversion in the gas phase never exceeds 0.01%. Therefore, unless special approaches are adopted to protect methanol, substantial efforts in direct methane conversion to obtain a high methanol yield will be in vain.

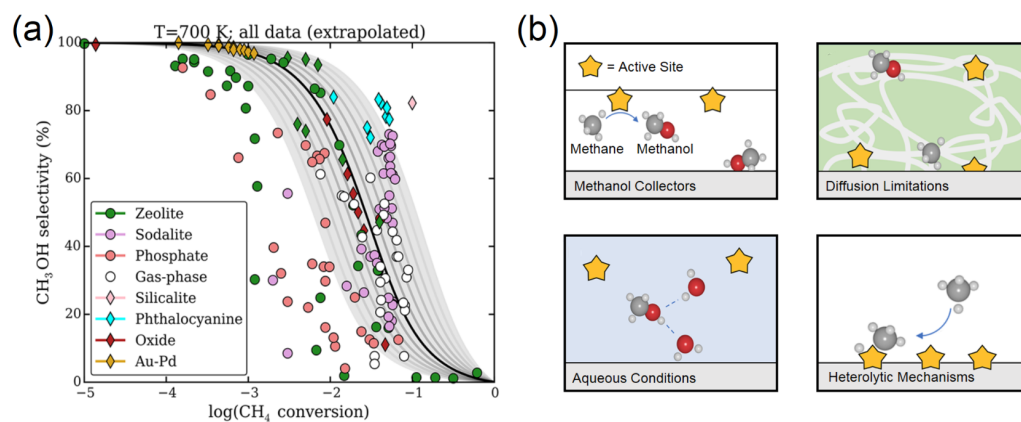


**Figure 14.** (a) Comparison of calculated and experimental methane conversion and methanol selectivity. (b) Protection strategies for methanol. Reprinted/adapted with permission from Ref. [87]. Copyright 2018, copyright American Chemical Society.

#### 4.2. Protection Strategies for Methanol in Continuous Reaction

Although the selectivity descriptor underscores how methane conversion is generally limited in continuous conversion, we summarize reasonable methods to break the selectivity limitations by considering the creation of new catalysts and processes. Breaking the limitations of methanol selectivity is similar to overcoming the inverse proportional linear relationship between activity with active species stability, namely introducing new variables [32,80] into the catalytic system to develop the conversion–selectivity balance in the expected direction. Several potential strategies have been suggested for protecting methanol (Figure 14b) by reducing  $\Delta G^{\ddagger}$  to achieve a higher methanol selectivity at the desired methane conversion rate.

Methanol “collectors” with a strong capability of adsorbing methanol can be utilized to avoid further methanol oxidation. The methanol “collectors” approach is adopted to reduce the partial pressure of methanol. For example, Palkovits et al. [88] stabilized the methyl group in the form of a methyl bisulfate intermediate in the methane conversion process. Subsequently, the methyl bisulfate intermediate was hydrolyzed to recover methanol, resulting in a methanol selectivity of >75%.

Aqueous conditions can be applied to stabilize methanol by liquid reaction solvents, mainly due to the difference in the solubility of the reactant methane and the product methanol. For example, Hutchings et al. [89] reported a one-step methane-to-methanol conversion using  $\text{H}_2\text{O}_2$  as an oxidant and Cu–Fe/ZSM-5 in a liquid medium. The methane conversion rate of the catalyst was 10.1%, and the methanol selectivity reached 93% at 50 °C. It was found that the non-framework dimer Fe species located on the internal surfaces of ZSM-5 served as the active site. Recently, the methanol selectivity of the single-site Ce–UiO–Co catalyst [90] reached 99% with  $\text{H}_2\text{O}_2$  as the oxidant in a liquid medium. As shown in Figure 15, Tang et al. [91] demonstrated that the C–H bond activation energy of methanol (1.34 eV) is ultimately greater than that of methane (1.16 eV) at the same Cu–O active site in the single-site  $\text{Cu}_1/\text{ZSM-5}$  catalyst, avoiding the overoxidation of methanol. This result is mainly due to different solvation contributions of methane and methanol under aqueous conditions. At the same time, higher methane pressures and lower methanol concentrations will further strengthen this trend, making methanol activation more difficult. Therefore, the liquid-phase environment in liquid–solid reactions plays a crucial role in improving methanol selectivity. It also explains the generally simultaneously higher methane conversion and methanol selectivity under aqueous conditions [92–94] than in gas-phase reactions [95–97] of the continuous methane-to-methanol conversion.

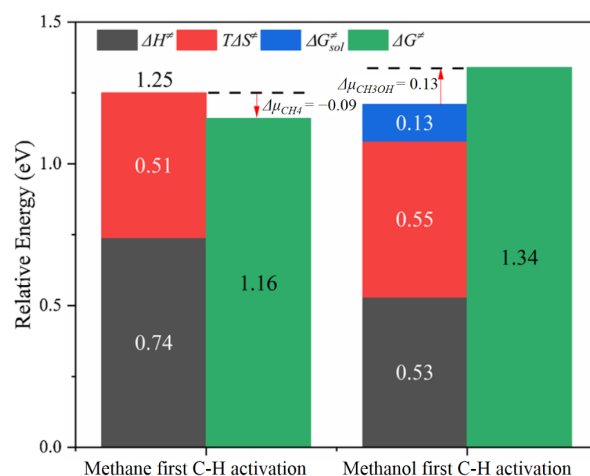


**Figure 15.** C–H bond activation free energies ( $\Delta G^{\ddagger}$ ) of methane and methanol.  $\Delta H^{\ddagger}$ ,  $T\Delta S^{\ddagger}$ , and  $\Delta G^{\ddagger}_{sol}$  as the contribution of enthalpy, entropy, and solvation, respectively.  $\Delta\mu$  is the pressure and concentration influence on  $\Delta G^{\ddagger}$ . Reprinted/adapted with permission from Ref. [91]. Copyright 2021, copyright Elsevier Ltd.

Diffusion-limited catalysts can be used to achieve enhanced methanol selectivity with a specific methane conversion rate. A diffusion-limited design has been realized in the fixation of AuPd alloy nanoparticles in ZSM-5 modified with hydrophobic organosilanes to encapsulate AuPd@ZSM-5 [98]. As shown in Figure 16, zeolite with a hydrophobic modification serving as a molecular fence only allows  $\text{CH}_4$ ,  $\text{O}_2$ , and  $\text{H}_2$  to access the AuPd active sites while limiting the diffusion of in situ generated  $\text{H}_2\text{O}_2$  around the AuPd active sites to enhance the reaction probability (I and II). Meanwhile, the formed methanol can quickly diffuse through the hydrophobic fence (III and IV). These modifications ultimately achieved a methane conversion of 17.3% with a 92% methanol selectivity at 70 °C. Recently, we also achieved efficient and stable direct methanol production from methane by hydrophobic Cu-BTC MOF catalysts [99].

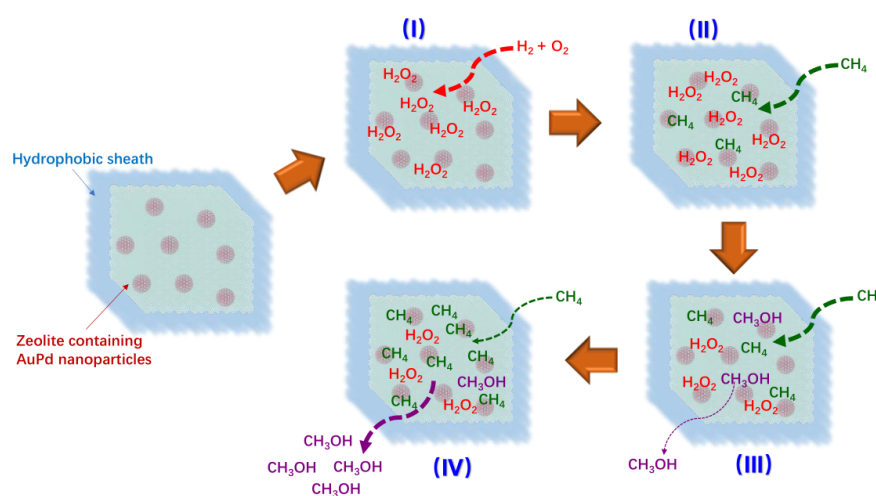


**Figure 16.** Scheme showing the molecular diffusion in hydrophobic AuPd@ZSM-5 for the direct oxidation-to-methanol conversion. Reprinted/adapted with permission from Ref. [98]. Copyright 2020, copyright American Association for the Advancement of Science.

Catalysts with methane activation via the heterolytic mechanism [45,100,101] remain a possible avenue to achieve a simultaneously high activity and selectivity, as investigations of the conversion–selectivity limit usually only consider active sites with methane activation via the homolytic mechanism. For example, Kwon et al. applied the single-atom Rh<sub>1</sub>-ZrO<sub>2</sub> catalyst [102] to achieve direct methane-to-methanol conversion. Figure 17a shows that the adsorbed CH<sub>3</sub> and H intermediates ( $\text{CH}_3^* + \text{H}^*$ ) in the Rh-O active sites have the lowest energy after the first C–H bond heterolytic breakage in the continuous activation of the methane conversion process. Therefore, the metal site on the catalyst surface can effectively stabilize the methyl group in the methane heterolytic mechanism, as compared to the generation of free methyl radicals in the homolytic mechanism. As another example, the CeO<sub>2</sub>/Cu<sub>2</sub>O interface [103] was found to directly convert methane to methanol with water and molecular oxygen at 450 K. During the reaction, the water-generated adsorbed hydroxyl species prevents O–O bond cleavage in molecular oxygen, as the formed oxygen species leads to the dehydrogenation of the methoxy group to carbon dioxide (Figure 17b). Furthermore, the hydroxyl species will directly bond with the methyl after methane activation to produce methanol (Figure 17c). Thus, water is the actual O-provider (more than 95% methanol), and molecular oxygen is mainly used to oxidize the reduced CeO<sub>2</sub> surface. Meanwhile, water also promotes methanol generation from the adsorbed \*CH<sub>3</sub>O species (Figure 17d). This group reported Cu<sub>2</sub>O as a support loading SnO [104] and ZnO [105] using the same strategy. These efforts represent a significant step in direct methane conversion to yield methanol using molecular oxygen with remarkable activity and selectivity.

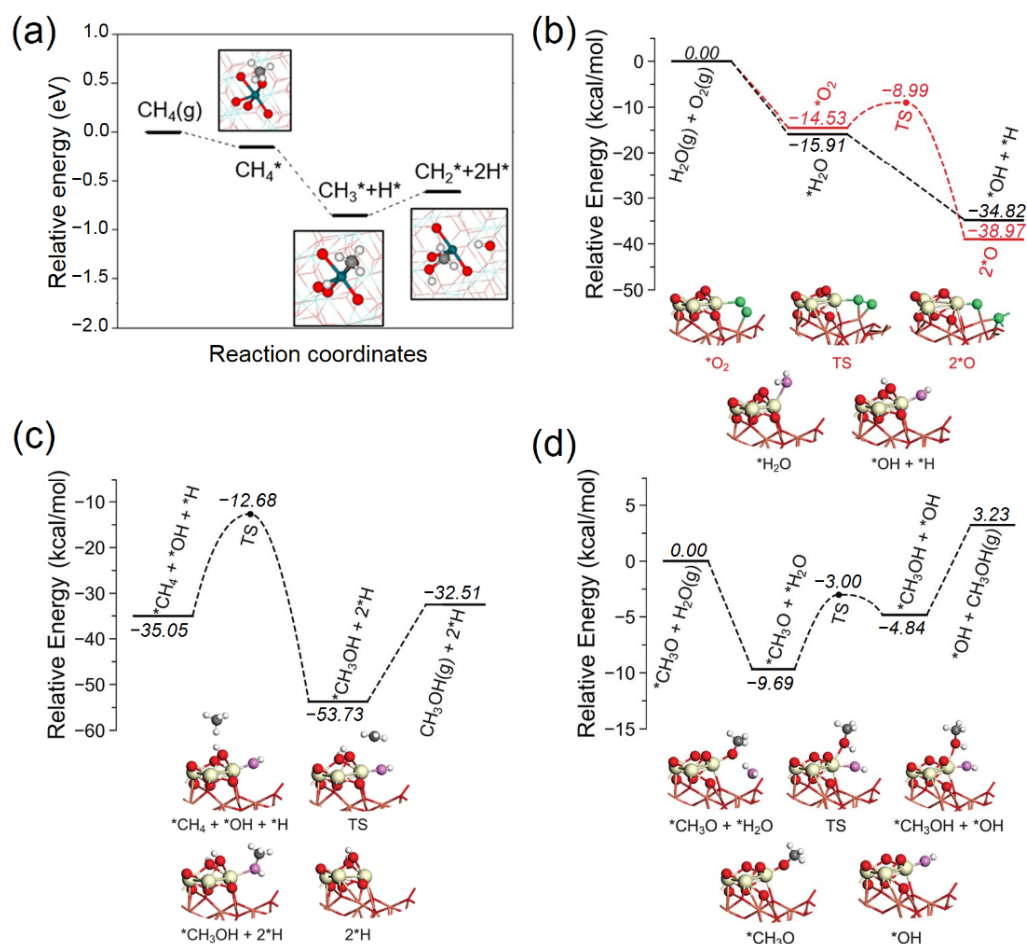


**Figure 17.** (a) Energy diagrams of continuous methane activation on Rh<sub>1</sub>/ZrO<sub>2</sub>. Reprinted/adapted with permission from Ref. [102]. Copyright 2017, copyright American Chemical Society. Reaction paths of three critical steps in direct methane-to-methanol conversion with oxygen and water on the interface of CeO<sub>2</sub>/Cu<sub>2</sub>O: (b) the water and oxygen dissociation (black and red, respectively), (c) the hydroxyl species from water to promote methane to methanol, and (d) the generation of methanol from the adsorbed \*CH<sub>3</sub>O species with the aid of water. Reprinted/adapted with permission from Ref. [103]. Copyright 2020, copyright American Association for the Advancement of Science.

#### 4.3. Stepwise Processes to Protect Methanol

In nature, methane monooxygenase enzymes overcome this challenge of conversion and selectivity by converting molecular oxygen and methane to methanol with an outstanding selectivity at ambient temperature and pressure, aided by flexible protein structures and gating mechanisms [85,106]. Inspired by the gating mechanism of biological enzymes [107] (Figure 18a), stepwise processes of oxidizing methane to methanol have been explored (Figure 18b), especially with zeolite [18] and MOF systems [108] in gas–solid reactions. The stepwise process involves three independent processes: active site formation by oxidants, methane activation, and methanol desorption with solvents.

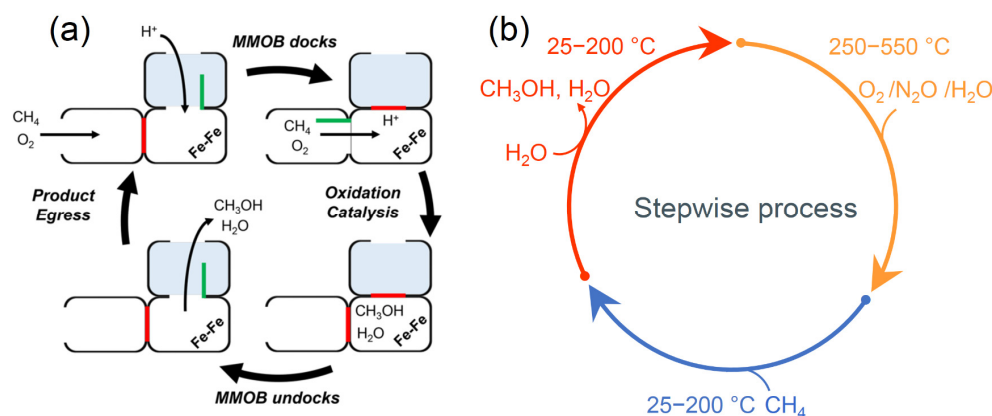


**Figure 18.** (a) Gating mechanism for direct methane-to-methanol conversion in methane monooxygenase enzymes' hydroxylase. Reprinted/adapted with permission from Ref. [107]. Copyright 2018, copyright American Chemical Society. (b) Independent optimization of the conditions of each stage in stepwise processes of direct methane-to-methanol conversion.

The spatial separation of the active species generation phase and the product formation phase in stepwise processes offers the inherent benefits of the effective stabilization of methyl species as an important intermediate in methanol. At the same time, methanol avoids encountering the newly generated active species in the next reaction cycle. Thus, the continued oxidation of desirable products (i.e., methanol) is prevented, resulting in an inherently higher selectivity compared to continuous processes in gas–solid reactions. For example, a high selectivity (~97%) over Cu-MOR [109] with dimer copper active sites can be achieved with stepwise processes in direct methane-to-methanol conversion. Meanwhile, using H<sub>2</sub>O as the oxidant (instead of H<sub>2</sub>O<sub>2</sub> [110] or N<sub>2</sub>O [37]) will promote the development of industrial processes for direct methane-to-methanol conversion.

However, in many stepwise catalysts, the desorption of methanol is extremely difficult and represents the rate-limiting step of the methane-to-methanol conversion [18]. Therefore, in stepwise processes, the ideal catalyst must have a moderate bonding energy to balance the two goals of simultaneously stabilizing the methyl group to protect methanol and achieving rapid methanol desorption under mild conditions. Meanwhile, to further improve the performance of stepwise processes for direct methane-to-methanol conversion, the choice of methanol extraction methods, desorption solvents, and reaction conditions [47] must be continuously optimized to reduce the switching time and energy consumption of different stages.

## 5. Perspectives

Although activity and selectivity descriptors can provide an initial optimization direction in the design and screening of catalysts, tremendous challenges remain in the further performance enhancement of direct methane-to-methanol conversion [3,111]. In view of these requirements, promising methods and technologies have emerged, providing new possibilities for efficient methane conversion across several different strategies.

### 5.1. The Synergistic Effect of Multicenter Active Sites

Cooperative active sites offer an opportunity to optimize the methane conversion performance. As shown in Figure 19a, the distant binuclear Fe(II) active sites in Fe-ferrierite [112] can achieve molecular dioxygen cleavage, and the two formed oxygen species (Fe(IV)=O) have a remarkable performance in direct methane-to-methanol conversion. Furthermore, active oxygen species are also formed over distant pairs of other M(II) (Co, Ni, and Mn) cations [113–115]. Arachchige et al. [116] demonstrated by DFT calculations that graphyne can confine single M (Fe, Co, Ni, and Cu) atoms. Two metal sites suitably distanced from each other in the adjacent pores of graphyne can interact simultaneously with molecular oxygen, where Fe@GY (Figure 19b) and Co@GY can effec-

tively promote oxygen activation to generate M–O active species for subsequent methane activation. Therefore, compared to a single active site, the synergistic effect in suitable multicenter active sites can efficiently activate molecular oxygen to reduce the activation energy of forming active species. Meanwhile, the reactive oxygen species are highly active, resulting in breaking existing relationships of the activity and the active species stability in single sites. This breakthrough has great practical importance in the development of prospective industrial catalysts in direct methane-to-methanol conversion.

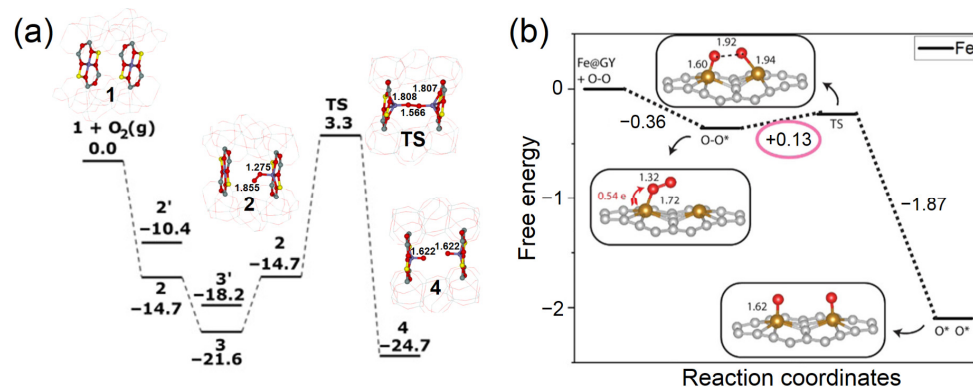


**Figure 19.** Reaction pathways of the  $O_2$  activation in (a) distant dinuclear Fe(II)-ferrierite (kcal/mol). Reprinted/adapted with permission from Ref. [112]. Copyright 2020, copyright American Association for the Advancement of Science. Reaction pathways of the  $O_2$  activation in (b) distant dinuclear Fe@GY. Reprinted/adapted with permission from Ref. [116]. Copyright 2021, copyright American Chemical Society.

### 5.2. Active Site Microenvironment

For the microenvironments of active sites, different local coordination and pore environments can offer diverse confinement effects, which will change the electronic properties of active centers and stabilize intermediates along reaction pathways to preserve a high activity and selectivity toward non- $CO_2$  products. For example, in Cu-MOR, Snyder et al. [117] proposed that the constricted region of the zeolite lattice will lead to closer van der Waals forces between methane and active sites, resulting in a lower activation energy, despite two dimer Cu active sites possessing similar electronic and geometric structures. The same group [118] also reported that although a single Fe in chabazite and beta zeolites (Fe-CHA and Fe-\*BEA) results in the identified active species  $\alpha$ -Fe(IV)=O and the local chemical environment, Fe-CHA had a significantly higher activity in recycle experiments. Experimental characterization and DFT calculations showed that the activity of different zeolites mainly depends on their pore size, where CHA (3.7 Å) has a smaller diffusion pore size compared to \*BEA (5.9 Å), and the van der Waals diameter of  $CH_4$  is 4.1–4.2 Å. Thus, Fe-CHA can effectively block the diffusion of  $\bullet CH_3$  radicals with an energy barrier of 5.2 kcal/mol after methane activation, and directly generate methanol through the  $\bullet CH_3$  rebound mechanism (the left side of Figure 20) with  $\alpha$ -Fe(III)-OH. Finally, the active sites in Fe-CHA can be regenerated after methanol desorption. However, Fe-BEA, with a larger pore size, has no hindered diffusion for the methyl radical. The methyl radical can freely diffuse to bond with other  $\alpha$ -Fe(IV)=O sites through the  $\bullet CH_3$  cage escape mechanism (the right side of Figure 20), making it unavailable for methane activation, whereas these active sites (i.e.,  $\alpha$ -Fe(III)-OCH<sub>3</sub> and  $\alpha$ -Fe(III)-OH) cannot be recovered. Therefore, the microenvironment plays a decisive role in producing different reaction pathways to regulate the performance of methane conversion, and strategies involving it are potentially broadly applicable in microporous materials [119].

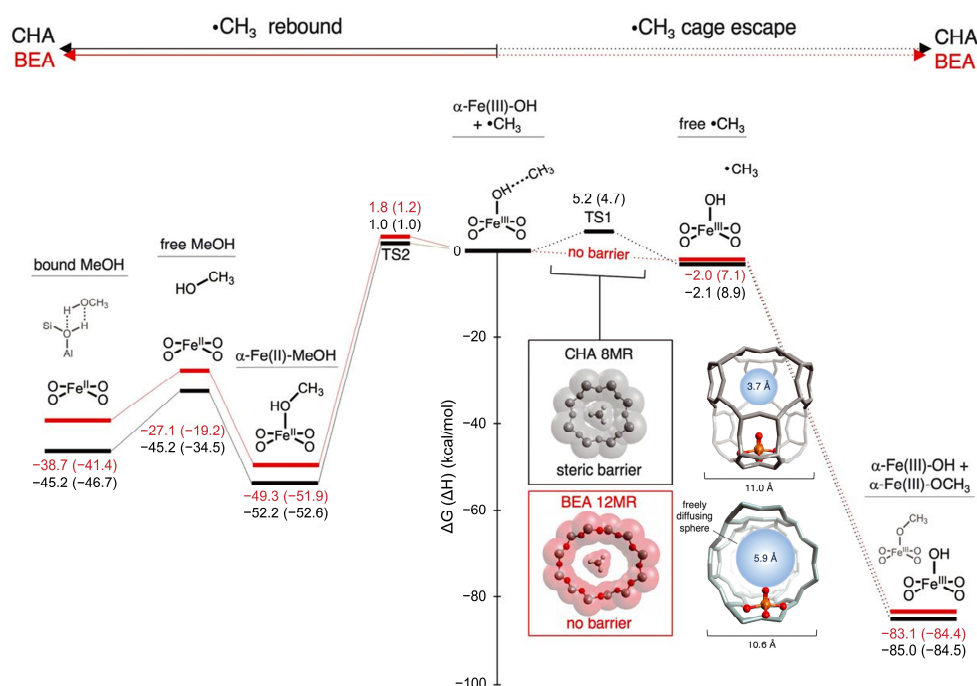


**Figure 20.** Comparison of reaction paths and CHA (black) and \*BEA (red) after the C–H bond activation in methane (kcal/mol). Reprinted/adapted with permission from Ref. [72]. Copyright 2021, copyright American Association for the Advancement of Science.

### 5.3. Co-Catalyst

In the presence of CO, Rh<sub>1</sub>-ZSM-5 [120,121] can achieve one-step methane activation to methanol and acetic acid using molecular oxygen as the oxidant in aqueous solutions at 150 °C, with a C1 selectivity exceeding 90%. Notably, even if CO is not directly involved in methanol formation, this process cannot be carried out without the addition of CO. Thus, monodispersed Rh(I)(CO)<sub>n</sub> species in the reaction can promote methane activation. In the overall reaction, as shown in Figure 21, CO plays a crucial role in the high catalytic performance [122]. It can be used as an oxidant to promote O<sub>2</sub> cleavage to generate Rh=O active species. At the same time, it can be used as a ligand of the Rh center to further reduce the methane activation energy. Subsequently, it can also act as a reactant to form acetic acid with the methyl group. Ir<sub>1</sub>-ZSM-5 [123] and Au/H-MOR [124] were proved to have similar reaction properties. Thus, this type of catalyst, with CO or other additives as co-catalysts, is worthy of further exploration to provide new ideas to design more efficient methane oxidation catalysts and processes.

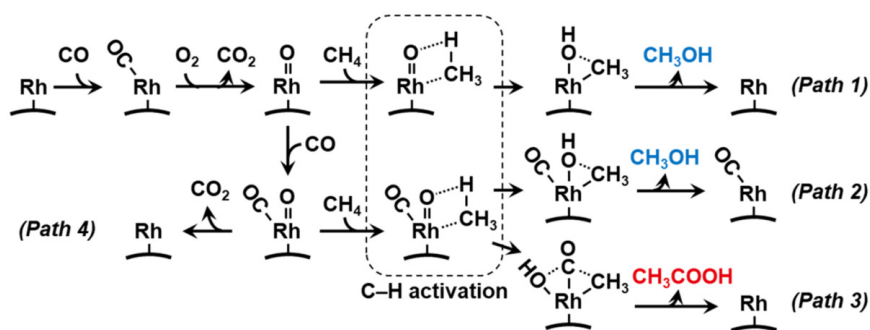


**Figure 21.** Reaction mechanisms of methane activation to methanol and acetic acid and the role of CO in Rh<sub>1</sub>-ZSM-5. Reprinted with permission from Ref. [122]. Copyright 2021, copyright Elsevier Ltd.

#### 5.4. Machine Learning-Assisted Techniques

Currently, the establishment of structure–reactivity relationships in experimental and theoretical results is mainly based on intuitive approaches with relatively low-density and low-dimensional information. With machine-learning (ML) methods [125,126], we can easily and quickly treat thousands of multiscale data using various mathematical models to automatically mine general and unique rules affecting catalytic performance. At the same time, standard workflows can be further established to screen huge samples with various features to obtain candidate catalysts at the lowest cost. Therefore, ML methods will accelerate the design of direct methane-to-methanol conversion catalysts.

The above-mentioned metal-oxo formation energy ( $E_f$ ) is a reactive descriptor of the methane conversion that is determined by a combination of various properties of metals, oxidation states, and ligands. Recently, Nandy et al. [30] applied large-scale computational screening through ML methods to accelerate the search for design rules in stable high-valent oxygen species via the input of 1200 open-shell and octahedral transition metal complexes with different features. The result showed that the stability of oxygen species is mainly determined by the metal type and non-local electronic ligand properties.

For the design of direct methane-to-methanol catalysts, as shown in Figure 22, Adamji et al. [127] developed a high-throughput screening workflow based on a MOF database (10,143 MOFs) and identified that certain MOFs with terminal metal-oxo species are synthesizable, thermally stable, and highly active toward methane. Subsequently, 87 MOFs meeting the initial screening criteria were further investigated with more detailed mechanistic studies. Finally, three Mn MOFs with weak-field ligands and curved/planar configurations showed remarkable kinetic and thermodynamic properties for the conversion of methane to methanol. Hence, ML-driven discovery can reveal design rules and provide a powerful screening strategy for methane conversion catalysts.

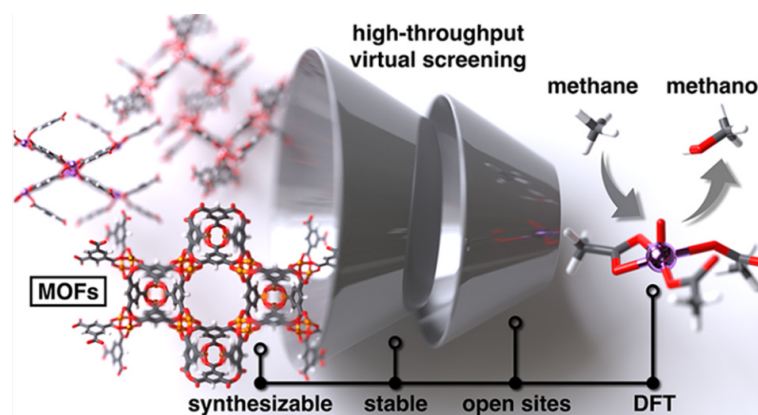


**Figure 22.** Computational discovery of MOF catalysts for direct methane-to-methanol conversion. Reprinted/adapted with permission from Ref. [127]. Copyright 2023, copyright American Chemical Society.

#### 5.5. Multicomponent Catalytic Materials

In converting methane to methanol, MOFs offer uniform active sites and versatile ligand structures to afford catalyst design with fine-tunable chemical properties [128,129], combining the characteristics of enzymes and homogeneous and heterogeneous catalysis. At the same time, certain MOFs have unique physical properties (e.g., high surface area and hydrophobicity [90]) that further improve catalytic performance in direct methane-to-methanol conversion. In addition to using MOFs alone [99], hydrophobic MOFs can also be used as the surface modification component on hydrophilic zeolites to form the two-component catalyst. Therein, zeolites realize the chemical process of methanol production from methane, and MOFs promote the physical process of methane adsorption and methanol desorption, avoiding strong interaction between methanol and hydrophilic

zeolites to improve the methanol selectivity. For example, Fe-ZSM-5@ZIF-8 [130] was proposed as a promising dual-component catalyst for direct methane-to-methanol conversion. In the reaction, methane adsorbs onto hydrophobic ZIF-8 and is subsequently activated by Fe-ZSM-5 to form methanol, whereas almost no methanol is produced in either Fe-ZSM-5 or ZIF-8 alone. Moreover, the hydrophobic ZIF-8 can promote the desorption of methanol. Therefore, the design of multicomponent catalytic systems incorporating materials with different physicochemical properties could make up for the shortcomings of traditional methane conversion materials.

### 5.6. Additional Energy Source

Recently developed reaction processes of methane conversion driven by electro- [48], plasma- [131], and photocatalysis [132] systems have been used in methane catalyst design. The additional energy input will reduce the temperature requirement of the catalytic reaction, significantly facilitating active species generation and methane activation [17] (Figure 23) to achieve direct methane conversion at room temperature using inexpensive oxidants. Thus, catalytic systems with various energy combinations have an opportunity to surpass the current limitations of thermal catalysis.

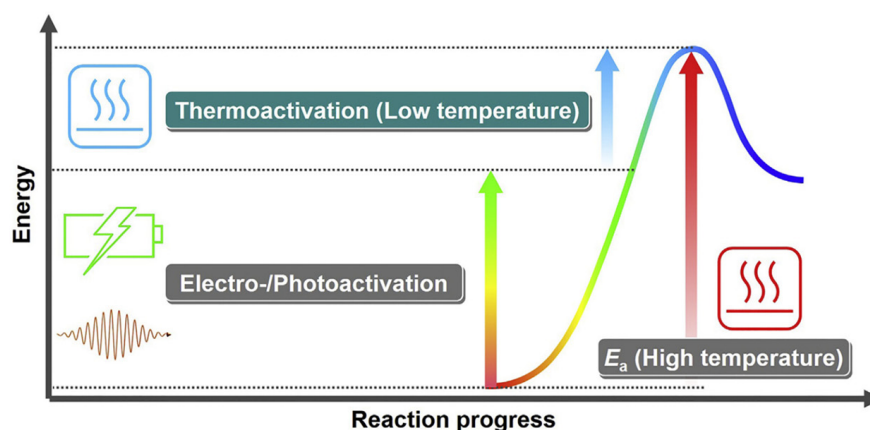


**Figure 23.** Diagram of methane activation energies in electro-/photocatalysts compared to thermal catalysts. Reprinted with permission from Ref. [17]. Copyright 2019 copyright Elsevier Ltd.

For example, the electrocatalyst CuO/CeO<sub>2</sub> [133] can directly convert methane to methanol with a production rate of 7165.0  $\mu\text{mol/gcat}$  in the presence of CO<sub>3</sub><sup>2-</sup> under ambient conditions. Fe/ $\gamma$ -Al<sub>2</sub>O<sub>3</sub> [134] has achieved single-step plasma-catalytic methane oxidation with O<sub>2</sub> with the oxygenate selectivity of 71.5% under ambient conditions. In the plasma gas-phase reaction, the critical CH<sub>x</sub> and OH species can be generated and combined to produce methanol. Au/ZnO [135], as an outstanding photocatalyst, achieved a C1 selectivity exceeding 95% under mild light irradiation using molecular oxygen in water at ambient temperature. This catalyst has the powerful ability to simultaneously activate methane and molecular oxygen to form  $\bullet\text{CH}_3$  and  $\bullet\text{OOH}$  radicals via photogenerated holes and electrons, resulting in the formation of liquid oxygenates and the suppression of overoxidation.

Owing to the limited development time of non-thermal catalysts of direct methane conversion, their active sites, reaction mechanisms, and the role of an external energy source remain largely unknown. However, these catalysts can generally use molecular oxygen to convert methane directly under ambient conditions, which is difficult to simultaneously achieve with current thermal catalysts. Therefore, using an additional energy source provides new possibilities for the design of catalysts to further promote the realization of industrialization in the direct conversion of methane to methanol under ambient conditions.

## 6. Conclusions

The direct oxidation of methane to methanol under ambient conditions has been regarded as the “holy grail” in the chemical community. To date, although immense efforts have been made, industrially viable catalysts and processes remain far from realization. However, with the aid of descriptors, it will be easier to discover promising material candidates and processes to simultaneously improve activity and selectivity. In this review, first, we classified the C–H activation of methane into two basic homolytic and heterolytic mechanisms and compared the characteristics of both active sites and reaction processes to provide a fundamental understanding of the methane activation of heterogeneous catalysts. Based on these two mechanisms, catalytic activity was evaluated using energy, electronic, and structural descriptors at the stages of methane activation and active species generation in direct methane-to-methanol conversion. Fundamentally, these descriptors all describe the active site’s ability to gain and lose electrons in the redox process from different dimensions. We further explain the moderate principle of descriptors in methane-to-methanol catalyst design and summarize related application work. Based on the activity descriptors, we summarized the underlying limitations of methane activation and active species generation, and provide different optimization strategies by introducing new variables with bond-breaking or bond-making events to overcome them. For methanol selectivity, a simple two-step selectivity model with a selectivity descriptor explains why the selectivity of continuous methane-to-methanol conversion is generally limited. Further, we provided strategies and principles to break the conversion–selectivity limit according to the characteristics of stepwise and continuous processes in direct methane-to-methanol conversion. Finally, based on pioneering work on the multiscale design of efficient catalysts for the direct oxidation of methane to methanol, further reasonable strategies are outlined, including the use of the synergistic effect of multiple active sites, the microenvironment of the active sites, co-catalysts, ML-assisted techniques, multicomponent catalytic materials, and additional energy sources. We hope to combine multiple variables to break the existing bottlenecks in direct methane-to-methanol conversion and simultaneously optimize methane conversion and methanol selectivity.

**Author Contributions:** Conceptualization, Z.Z.; methodology, W.S., B.L. and Z.Z.; investigation, Z.L.; resources, Z.Z.; data curation, Z.L., Y.C. and Z.X.; writing—original draft preparation, Z.L.; writing—review and editing, W.S., B.L. and Z.Z.; visualization, Z.L., Y.C. and Z.X.; supervision, W.S., B.L. and Z.Z.; project administration, Z.Z.; funding acquisition, Z.Z. All authors have read and agreed to the published version of the manuscript.

**Funding:** This work was financially supported by the major research projects of the National Natural Science Foundation of China (No. 92145301, 91845201, and 22102106).

**Data Availability Statement:** Not applicable.

**Conflicts of Interest:** The authors declare no conflict of interest.

## References

1. Nkinahamira, F.; Yang, R.; Zhu, R.; Zhang, J.; Ren, Z.; Sun, S.; Xiong, H.; Zeng, Z. Current Progress on Methods and Technologies for Catalytic Methane Activation at Low Temperatures. *Adv. Sci.* **2023**, *10*, 2204566. [[CrossRef](#)] [[PubMed](#)]
2. Tomkins, P.; Ranocchiari, M.; van Bokhoven, J.A. Direct Conversion of Methane to Methanol under Mild Conditions over Cu-Zeolites and Beyond. *Acc. Chem. Res.* **2017**, *50*, 418–425. [[CrossRef](#)] [[PubMed](#)]
3. Srivastava, R.K.; Sarangi, P.K.; Bhatia, L.; Singh, A.K.; Shadangi, K.P. Conversion of Methane to Methanol: Technologies and Future Challenges. *Biomass Conv. Bioref.* **2022**, *12*, 1851–1875. [[CrossRef](#)]
4. Freakley, S.J.; Dimitratos, N.; Willock, D.J.; Taylor, S.H.; Kiely, C.J.; Hutchings, G.J. Methane Oxidation to Methanol in Water. *Acc. Chem. Res.* **2021**, *54*, 2614–2623. [[CrossRef](#)] [[PubMed](#)]
5. Dummer, N.F.; Willock, D.J.; He, Q.; Howard, M.J.; Lewis, R.J.; Qi, G.; Taylor, S.H.; Xu, J.; Bethell, D.; Kiely, C.J.; et al. Methane Oxidation to Methanol. *Chem. Rev.* **2023**, *123*, 6359–6411. [[CrossRef](#)] [[PubMed](#)]
6. Cui, X.; Huang, R.; Deng, D. Catalytic Conversion of C1 Molecules under Mild Conditions. *EnergyChem* **2021**, *3*, 100050. [[CrossRef](#)]
7. Yu, T.; Li, Z.; Lin, L.; Chu, S.; Su, Y.; Song, W.; Wang, A.; Weckhuysen, B.M.; Luo, W. Highly Selective Oxidation of Methane into Methanol over Cu-Promoted Monomeric Fe/ZSM-5. *ACS Catal.* **2021**, *11*, 6684–6691. [[CrossRef](#)]

8. Yu, T.; Li, Z.; Jones, W.; Liu, Y.; He, Q.; Song, W.; Du, P.; Yang, B.; An, H.; Farmer, D.M.; et al. Identifying Key Mononuclear Fe Species for Low-Temperature Methane Oxidation. *Chem. Sci.* **2021**, *12*, 3152–3160. [[CrossRef](#)]
9. Kumar, P.; Al-Attas, T.A.; Hu, J.; Kibria, M.G. Single Atom Catalysts for Selective Methane Oxidation to Oxygenates. *ACS Nano* **2022**, *16*, 8557–8618. [[CrossRef](#)]
10. Newton, M.A.; Knorpp, A.J.; Sushkevich, V.L.; Palagin, D.; Van Bokhoven, J.A. Active Sites and Mechanisms in the Direct Conversion of Methane to Methanol Using Cu in Zeolitic Hosts: A Critical Examination. *Chem. Soc. Rev.* **2020**, *49*, 1449–1486. [[CrossRef](#)]
11. Wei, Y.-S.; Zhang, M.; Zou, R.; Xu, Q. Metal–Organic Framework-Based Catalysts with Single Metal Sites. *Chem. Rev.* **2020**, *120*, 12089–12174. [[CrossRef](#)] [[PubMed](#)]
12. Yang, N.; Zhao, Y.; Wu, P.; Liu, G.; Sun, F.; Ma, J.; Jiang, Z.; Sun, Y.; Zeng, G. Defective C<sub>3</sub>N<sub>4</sub> Frameworks Coordinated Diatomic Copper Catalyst: Towards Mild Oxidation of Methane to C1 Oxygenates. *Appl. Catal. B* **2021**, *299*, 120682. [[CrossRef](#)]
13. Fan, J.; Liang, S.; Zhu, K.; Mao, J.; Cui, X.; Ma, C.; Yu, L.; Deng, D. Boosting Room-Temperature Conversion of Methane via Confining Cu Atoms in Ultrathin Ru Nanosheets. *Chem. Catal.* **2022**, *2*, 2253–2261. [[CrossRef](#)]
14. Liu, H.; Kang, L.; Wang, H.; Jiang, Q.; Liu, X.Y.; Wang, A. Ru Single-Atom Catalyst Anchored on Sulfated Zirconia for Direct Methane Conversion to Methanol. *Chin. J. Catal.* **2023**, *46*, 64–71. [[CrossRef](#)]
15. Bai, S.; Liu, F.; Huang, B.; Li, F.; Lin, H.; Wu, T.; Sun, M.; Wu, J.; Shao, Q.; Xu, Y.; et al. High-Efficiency Direct Methane Conversion to Oxygenates on a Cerium Dioxide Nanowires Supported Rhodium Single-Atom Catalyst. *Nat. Commun.* **2020**, *11*, 954. [[CrossRef](#)]
16. Sharma, R.; Poelman, H.; Marin, G.B.; Galvita, V.V. Approaches for Selective Oxidation of Methane to Methanol. *Catalysts* **2020**, *10*, 194. [[CrossRef](#)]
17. Meng, X.; Cui, X.; Rajan, N.P.; Yu, L.; Deng, D.; Bao, X. Direct Methane Conversion under Mild Condition by Thermo-, Electro-, or Photocatalysis. *Chem* **2019**, *5*, 2296–2325. [[CrossRef](#)]
18. Mahyuddin, M.H.; Shiota, Y.; Yoshizawa, K. Methane Selective Oxidation to Methanol by Metal-Exchanged Zeolites: A Review of Active Sites and Their Reactivity. *Catal. Sci. Technol.* **2019**, *9*, 1744–1768. [[CrossRef](#)]
19. Seh, Z.W.; Kibsgaard, J.; Dickens, C.F.; Chorkendorff, I.; Nørskov, J.K.; Jaramillo, T.F. Combining Theory and Experiment in Electrocatalysis: Insights into Materials Design. *Science* **2017**, *355*, eaad4998. [[CrossRef](#)]
20. Su, H.-Y.; Sun, K.; Wang, W.-Q.; Zeng, Z.; Calle-Vallejo, F.; Li, W.-X. Establishing and Understanding Adsorption-Energy Scaling Relations with Negative Slopes. *J. Phys. Chem. Lett.* **2016**, *7*, 5302–5306. [[CrossRef](#)]
21. Zheng, H.; Li, R.; Zhong, C.; Li, Z.; Kang, Y.; Deng, J.; Song, W.; Zhao, Z. Theoretical Design of Transition Metal-Doped TiO<sub>2</sub> for the Selective Catalytic Reduction of NO with NH<sub>3</sub> by DFT Calculations. *Catal. Sci. Technol.* **2022**, *12*, 1429–1440. [[CrossRef](#)]
22. Zhao, Z.-J.; Liu, S.; Zha, S.; Cheng, D.; Studt, F.; Henkelman, G.; Gong, J. Theory-Guided Design of Catalytic Materials Using Scaling Relationships and Reactivity Descriptors. *Nat. Rev. Mater.* **2019**, *4*, 792–804. [[CrossRef](#)]
23. Jia, C.; Wang, Q.; Yang, J.; Ye, K.; Li, X.; Zhong, W.; Shen, H.; Sharman, E.; Luo, Y.; Jiang, J. Toward Rational Design of Dual-Metal-Site Catalysts: Catalytic Descriptor Exploration. *ACS Catal.* **2022**, *12*, 3420–3429. [[CrossRef](#)]
24. Seemakurthi, R.R.; Canning, G.; Wu, Z.; Miller, J.T.; Datye, A.K.; Greeley, J. Identification of a Selectivity Descriptor for Propane Dehydrogenation through Density Functional and Microkinetic Analysis on Pure Pd and Pd Alloys. *ACS Catal.* **2021**, *11*, 9588–9604. [[CrossRef](#)]
25. Chen, S.; Zaffran, J.; Yang, B. Descriptor Design in the Computational Screening of Ni-Based Catalysts with Balanced Activity and Stability for Dry Reforming of Methane Reaction. *ACS Catal.* **2020**, *10*, 3074–3083. [[CrossRef](#)]
26. Xie, Z.; Li, Z.; Tang, P.; Song, Y.; Zhao, Z.; Kong, L.; Fan, X.; Xiao, X. The Effect of Oxygen Vacancies on the Coordinatively Unsaturated Al-O Acid-Base Pairs for Propane Dehydrogenation. *J. Catal.* **2021**, *397*, 172–182. [[CrossRef](#)]
27. Yu, T.; Li, Z.; Zheng, H.; Chen, L.; Song, W.; Zhao, Z.; Li, J.; Liu, J. The Nature of Ni-O Pairs for Ethane Activation on NiO(100) and NiO(110) Surfaces. *Mol. Catal.* **2019**, *474*, 110417. [[CrossRef](#)]
28. Singh, A.R.; Montoya, J.H.; Rohr, B.A.; Tsai, C.; Vojvodic, A.; Nørskov, J.K. Computational Design of Active Site Structures with Improved Transition-State Scaling for Ammonia Synthesis. *ACS Catal.* **2018**, *8*, 4017–4024. [[CrossRef](#)]
29. Nørskov, J.K.; Bligaard, T.; Rossmeisl, J.; Christensen, C.H. Towards the Computational Design of Solid Catalysts. *Nat. Chem.* **2009**, *1*, 37–46. [[CrossRef](#)]
30. Nandy, A.; Zhu, J.; Janet, J.P.; Duan, C.; Getman, R.B.; Kulik, H.J. Machine Learning Accelerates the Discovery of Design Rules and Exceptions in Stable Metal–Oxo Intermediate Formation. *ACS Catal.* **2019**, *9*, 8243–8255. [[CrossRef](#)]
31. Gani, T.Z.H.; Kulik, H.J. Understanding and Breaking Scaling Relations in Single-Site Catalysis: Methane to Methanol Conversion by Fe<sup>IV</sup>=O. *ACS Catal.* **2018**, *8*, 975–986. [[CrossRef](#)]
32. Pérez-Ramírez, J.; López, N. Strategies to Break Linear Scaling Relationships. *Nat. Catal.* **2019**, *2*, 971–976. [[CrossRef](#)]
33. Doan, H.A.; Wang, X.; Snurr, R.Q. Computational Screening of Supported Metal Oxide Nanoclusters for Methane Activation: Insights into Homolytic versus Heterolytic C–H Bond Dissociation. *J. Phys. Chem. Lett.* **2023**, *14*, 5018–5024. [[CrossRef](#)] [[PubMed](#)]
34. Olivos-Suarez, A.I.; Szécsényi, Á.; Hensen, E.J.M.; Ruiz-Martinez, J.; Pidko, E.A.; Gascon, J. Strategies for the Direct Catalytic Valorization of Methane Using Heterogeneous Catalysis: Challenges and Opportunities. *ACS Catal.* **2016**, *6*, 2965–2981. [[CrossRef](#)]
35. Mahyuddin, M.H.; Shiota, Y.; Staykov, A.; Yoshizawa, K. Theoretical Investigation of Methane Hydroxylation over Isoelectronic [FeO]<sup>2+</sup>- and [MnO]<sup>+</sup>-Exchanged Zeolites Activated by N<sub>2</sub>O. *Inorg. Chem.* **2017**, *56*, 10370–10380. [[CrossRef](#)]

36. Szécsényi, Á.; Li, G.; Gascon, J.; Pidko, E.A. Unraveling Reaction Networks behind the Catalytic Oxidation of Methane with  $\text{H}_2\text{O}_2$  over a Mixed-Metal MIL-53(Al,Fe) MOF Catalyst. *Chem. Sci.* **2018**, *9*, 6765–6773. [[CrossRef](#)]
37. Snyder, B.E.R.; Vanelderen, P.; Bols, M.L.; Hallaert, S.D.; Böttger, L.H.; Ungur, L.; Pierloot, K.; Schoonheydt, R.A.; Sels, B.F.; Solomon, E.I. The Active Site of Low-Temperature Methane Hydroxylation in Iron-Containing Zeolites. *Nature* **2016**, *536*, 317–321. [[CrossRef](#)]
38. Zhu, K.; Liang, S.; Cui, X.; Huang, R.; Wan, N.; Hua, L.; Li, H.; Chen, H.; Zhao, Z.; Hou, G.; et al. Highly Efficient Conversion of Methane to Formic Acid under Mild Conditions at ZSM-5-Confined Fe-Sites. *Nano Energy* **2021**, *82*, 105718. [[CrossRef](#)]
39. Barona, M.; Snurr, R.Q. Exploring the Tunability of Trimetallic Mof Nodes for Partial Oxidation of Methane to Methanol. *ACS Appl. Mater. Interfaces* **2020**, *12*, 28217–28231. [[CrossRef](#)]
40. Ravi, M.; Ranocchiari, M.; van Bokhoven, J.A. The Direct Catalytic Oxidation of Methane to Methanol—A Critical Assessment. *Angew. Chem. Int. Ed.* **2017**, *56*, 16464–16483. [[CrossRef](#)]
41. Senanayake, S.D.; Rodriguez, J.A.; Weaver, J.F. Low Temperature Activation of Methane on Metal-Oxides and Complex Interfaces: Insights from Surface Science. *Acc. Chem. Res.* **2020**, *53*, 1488–1497. [[CrossRef](#)] [[PubMed](#)]
42. Liang, Z.; Li, T.; Kim, M.; Asthagiri, A.; Weaver, J.F. Low-Temperature Activation of Methane on the  $\text{IrO}_2(110)$  Surface. *Science* **2017**, *356*, 299–303. [[CrossRef](#)] [[PubMed](#)]
43. Latimer, A.A.; Aljama, H.; Kakekhani, A.; Yoo, J.S.; Kulkarni, A.; Tsai, C.; Garcia-Melchor, M.; Abild-Pedersen, F.; Nørskov, J.K. Mechanistic Insights into Heterogeneous Methane Activation. *Phys. Chem. Chem. Phys.* **2017**, *19*, 3575–3581. [[CrossRef](#)]
44. Szécsényi, Á.; Li, G.; Gascon, J.; Pidko, E.A. Mechanistic Complexity of Methane Oxidation with  $\text{H}_2$  by Single-Site Fe/ZSM-5 Catalyst. *ACS Catal.* **2018**, *8*, 7961–7972. [[CrossRef](#)] [[PubMed](#)]
45. Yang, L.; Huang, J.; Ma, R.; You, R.; Zeng, H.; Rui, Z. Metal–Organic Framework-Derived  $\text{IrO}_2/\text{CuO}$  Catalyst for Selective Oxidation of Methane to Methanol. *ACS Energy Lett.* **2019**, *4*, 2945–2951. [[CrossRef](#)]
46. Zhou, Y.; Zhang, L.; Wang, W. Direct Functionalization of Methane into Ethanol over Copper Modified Polymeric Carbon Nitride via Photocatalysis. *Nat. Commun.* **2019**, *10*, 506. [[CrossRef](#)]
47. Ravi, M.; Sushkevich, V.L.; Knorpp, A.J.; Newton, M.A.; Palagin, D.; Pinar, A.B.; Ranocchiari, M.; van Bokhoven, J.A. Misconceptions and Challenges in Methane-to-Methanol over Transition-Metal-Exchanged Zeolites. *Nat. Catal.* **2019**, *2*, 485–494. [[CrossRef](#)]
48. Yuan, S.; Li, Y.; Peng, J.; Questell-Santiago, Y.M.; Akkiraju, K.; Giordano, L.; Zheng, D.J.; Bagi, S.; Román-Leshkov, Y.; Shao-Horn, Y. Conversion of Methane into Liquid Fuels—Bridging Thermal Catalysis with Electrocatalysis. *Adv. Energy Mater.* **2020**, *10*, 2002154. [[CrossRef](#)]
49. Wang, Y.; Hu, P.; Yang, J.; Zhu, Y.-A.; Chen, D. C–H Bond Activation in Light Alkanes: A Theoretical Perspective. *Chem. Soc. Rev.* **2021**, *50*, 4299–4358. [[CrossRef](#)]
50. Wang, G.; Huang, L.; Chen, W.; Zhou, J.; Zheng, A. Rationally Designing Mixed Cu–( $\mu$ -O)–M (M = Cu, Ag, Zn, Au) Centers over Zeolite Materials with High Catalytic Activity towards Methane Activation. *Phys. Chem. Chem. Phys.* **2018**, *20*, 26522–26531. [[CrossRef](#)]
51. Wang, L.; Li, Z.; Wang, Z.; Chen, X.; Song, W.; Zhao, Z.; Wei, Y.; Zhang, X. Hetero-Metallic Active Sites in Omega (MAZ) Zeolite-Catalyzed Methane Partial Oxidation: A DFT Study. *Ind. Eng. Chem. Res.* **2021**, *60*, 2400–2409. [[CrossRef](#)]
52. Ma, D.; Cao, X.; Cao, Z. Selective Oxidation of  $\text{CH}_4$  to  $\text{CH}_3\text{OH}$  by Transition-Metal Single-Atom-Embedded N-Doped Graphene Catalysts with Oxidants  $\text{N}_2\text{O}$  and  $\text{O}_2$ : Oxygen Adsorption Energy as an Activity Descriptor. *J. Phys. Chem. C* **2023**, *127*, 5800–5809. [[CrossRef](#)]
53. Ganai, A.; Ball, B.; Sarkar, P. Modulating the Energetics of C–H Bond Activation in Methane by Utilizing Metalated Porphyrinic Metal–Organic Frameworks. *J. Phys. Chem. Lett.* **2023**, *14*, 1832–1839. [[CrossRef](#)] [[PubMed](#)]
54. Bligaard, T.; Nørskov, J.K.; Dahl, S.; Matthiesen, J.; Christensen, C.H.; Sehested, J. The Brønsted–Evans–Polanyi Relation and the Volcano Curve in Heterogeneous Catalysis. *J. Catal.* **2004**, *224*, 206–217. [[CrossRef](#)]
55. Latimer, A.A.; Kulkarni, A.R.; Aljama, H.; Montoya, J.H.; Yoo, J.S.; Tsai, C.; Abild-Pedersen, F.; Studt, F.; Nørskov, J.K. Understanding Trends in C–H Bond Activation in Heterogeneous Catalysis. *Nat. Mater.* **2017**, *16*, 225–229. [[CrossRef](#)] [[PubMed](#)]
56. Mahyuddin, M.H.; Shiota, Y.; Staykov, A.; Yoshizawa, K. Theoretical Overview of Methane Hydroxylation by Copper–Oxygen Species in Enzymatic and Zeolitic Catalysts. *Acc. Chem. Res.* **2018**, *51*, 2382–2390. [[CrossRef](#)]
57. Grundner, S.; Markovits, M.A.C.; Li, G.; Tromp, M.; Pidko, E.A.; Hensen, E.J.M.; Jentys, A.; Sanchez-Sanchez, M.; Lercher, J.A. Single-Site Trinuclear Copper Oxygen Clusters in Mordenite for Selective Conversion of Methane to Methanol. *Nat. Commun.* **2015**, *6*, 7546. [[CrossRef](#)]
58. Kumar, G.; Lau, S.L.J.; Krcha, M.D.; Janik, M.J. Correlation of Methane Activation and Oxide Catalyst Reducibility and Its Implications for Oxidative Coupling. *ACS Catal.* **2016**, *6*, 1812–1821. [[CrossRef](#)]
59. Fung, V.; Tao, F.; Jiang, D. Low-Temperature Activation of Methane on Doped Single Atoms: Descriptor and Prediction. *Phys. Chem. Chem. Phys.* **2018**, *20*, 22909–22914. [[CrossRef](#)]
60. Liu, C.; Li, G.; Pidko, E.A. Property–Activity Relations for Methane Activation by Dual-metal Cu–Oxo Trimers in ZSM-5 Zeolite. *Small Methods* **2018**, *2*, 1800266. [[CrossRef](#)]
61. Zheng, J.; Ye, J.; Ortuño, M.A.; Fulton, J.L.; Gutiérrez, O.Y.; Camaioni, D.M.; Motkuri, R.K.; Li, Z.; Webber, T.E.; Mehdi, B.L.; et al. Selective Methane Oxidation to Methanol on Cu–Oxo Dimers Stabilized by Zirconia Nodes of an NU-1000 Metal–Organic Framework. *J. Am. Chem. Soc.* **2019**, *141*, 9292–9304. [[CrossRef](#)] [[PubMed](#)]

62. Mahyuddin, M.H.; Tanaka, T.; Shiota, Y.; Staykov, A.; Yoshizawa, K. Methane Partial Oxidation over  $[\text{Cu}_2(\mu\text{-O})]^{2+}$  and  $[\text{Cu}_3(\mu\text{-O})_3]^{2+}$  Active Species in Large-Pore Zeolites. *ACS Catal.* **2018**, *8*, 1500–1509. [\[CrossRef\]](#)
63. Rosen, A.S.; Notestein, J.M.; Snurr, R.Q. Structure–Activity Relationships That Identify Metal–Organic Framework Catalysts for Methane Activation. *ACS Catal.* **2019**, *9*, 3576–3587. [\[CrossRef\]](#)
64. Filonowich, D.; Luna, M.; Quinn, T.; Choudhury, P. Electronic Descriptor of Single Metal-Oxo Species on Phthalocyanine- and Porphyrin-Functionalized Graphene toward Methane Activation Process. *J. Phys. Chem. C* **2020**, *124*, 4502–4510. [\[CrossRef\]](#)
65. Zha, S.; Zhao, Z.-J.; Chen, S.; Liu, S.; Liu, T.; Studt, F.; Gong, J. Predicting the Catalytic Activity of Surface Oxidation Reactions by Ionization Energies. *CCS Chem.* **2020**, *2*, 262–270. [\[CrossRef\]](#)
66. Xu, J.; Cao, X.-M.; Hu, P. Improved Prediction for the Methane Activation Mechanism on Rutile Metal Oxides by a Machine Learning Model with Geometrical Descriptors. *J. Phys. Chem. C* **2019**, *123*, 28802–28810. [\[CrossRef\]](#)
67. Mahyuddin, M.H.; Staykov, A.; Shiota, Y.; Miyanishi, M.; Yoshizawa, K. Roles of Zeolite Confinement and Cu–O–Cu Angle on the Direct Conversion of Methane to Methanol by  $[\text{Cu}_2(\mu\text{-O})]^{2+}$ -Exchanged Aei, Cha, Afx, and Mfi Zeolites. *ACS Catal.* **2017**, *7*, 3741–3751. [\[CrossRef\]](#)
68. Fung, V.; Tao, F.F.; Jiang, D. General Structure–Reactivity Relationship for Oxygen on Transition-Metal Oxides. *J. Phys. Chem. Lett.* **2017**, *8*, 2206–2211. [\[CrossRef\]](#)
69. Nørskov, J.K.; Abild-Pedersen, F.; Studt, F.; Bligaard, T. Density Functional Theory in Surface Chemistry and Catalysis. *Proc. Natl. Acad. Sci. USA* **2011**, *108*, 937–943. [\[CrossRef\]](#)
70. Jiao, S.; Fu, X.; Huang, H. Descriptors for the Evaluation of Electrocatalytic Reactions: D-Band Theory and Beyond. *Adv. Funct. Mater.* **2022**, *32*, 2107651. [\[CrossRef\]](#)
71. Hammer, B.; Nørskov, J.K. Why Gold Is the Noblest of All the Metals. *Nature* **1995**, *376*, 238–240. [\[CrossRef\]](#)
72. Medford, A.J.; Vojvodic, A.; Hummelshøj, J.S.; Voss, J.; Abild-Pedersen, F.; Studt, F.; Bligaard, T.; Nilsson, A.; Nørskov, J.K. From the Sabatier Principle to a Predictive Theory of Transition-Metal Heterogeneous Catalysis. *J. Catal.* **2015**, *328*, 36–42. [\[CrossRef\]](#)
73. Choi, C.; Yoon, S.; Jung, Y. Shifting the Scaling Relations of Single-Atom Catalysts for Facile Methane Activation by Tuning the Coordination Number. *Chem. Sci.* **2021**, *12*, 3551–3557. [\[CrossRef\]](#) [\[PubMed\]](#)
74. Cui, X.; Li, H.; Wang, Y.; Hu, Y.; Hua, L.; Li, H.; Han, X.; Liu, Q.; Yang, F.; He, L.; et al. Room-Temperature Methane Conversion by Graphene-Confined Single Iron Atoms. *Chem* **2018**, *4*, 1902–1910. [\[CrossRef\]](#)
75. Tan, X.; Tahini, H.A.; Smith, S.C. Defect Engineering in Graphene-Confined Single-Atom Iron Catalysts for Room-Temperature Methane Conversion. *J. Phys. Chem. C* **2021**, *125*, 12628–12635. [\[CrossRef\]](#)
76. Kulkarni, A.R.; Zhao, Z.-J.; Siahrostami, S.; Nørskov, J.K.; Studt, F. Cation-Exchanged Zeolites for the Selective Oxidation of Methane to Methanol. *Catal. Sci. Technol.* **2018**, *8*, 114–123. [\[CrossRef\]](#)
77. Wang, S.; Xin, Y.; Yuan, J.; Wang, L.; Zhang, W. Direct Conversion of Methane to Methanol on Boron Nitride-Supported Copper Single Atoms. *Nanoscale* **2022**, *14*, 5447–5453. [\[CrossRef\]](#)
78. Kang, Y.; Li, Z.; Lv, X.; Song, W.; Wei, Y.; Zhang, X.; Liu, J.; Zhao, Z. Active Oxygen Promoted Electrochemical Conversion of Methane on Two-Dimensional Carbide (MXenes): From Stability, Reactivity and Selectivity. *J. Catal.* **2021**, *393*, 20–29. [\[CrossRef\]](#)
79. Szécsényi, Á.; Khramenkova, E.; Chernyshov, I.Y.; Li, G.; Gascon, J.; Pidko, E.A. Breaking Linear Scaling Relationships with Secondary Interactions in Confined Space: A Case Study of Methane Oxidation by Fe/ZSM-5 Zeolite. *ACS Catal.* **2019**, *9*, 9276–9284. [\[CrossRef\]](#)
80. Jeong, H.; Shin, S.; Lee, H. Heterogeneous Atomic Catalysts Overcoming the Limitations of Single-Atom Catalysts. *ACS Nano* **2020**, *14*, 14355–14374. [\[CrossRef\]](#)
81. Brozek, C.K.; Dincă, M.  $\text{Ti}^{3+}$ -,  $\text{V}^{2+/3+}$ -,  $\text{Cr}^{2+/3+}$ -,  $\text{Mn}^{2+}$ -, and  $\text{Fe}^{2+}$ -Substituted MOF-5 and Redox Reactivity in Cr- and Fe-MOF-5. *J. Am. Chem. Soc.* **2013**, *135*, 12886–12891. [\[CrossRef\]](#) [\[PubMed\]](#)
82. Göttl, F.; Michel, C.; Andrikopoulos, P.C.; Love, A.M.; Hafner, J.; Hermans, I.; Sautet, P. Computationally Exploring Confinement Effects in the Methane-to-Methanol Conversion Over Iron-Oxo Centers in Zeolites. *ACS Catal.* **2016**, *6*, 8404–8409. [\[CrossRef\]](#)
83. Valvekens, P.; Vermoortele, F.; De Vos, D. Metal–Organic Frameworks as Catalysts: The Role of Metal Active Sites. *Catal. Sci. Technol.* **2013**, *3*, 1435. [\[CrossRef\]](#)
84. Vitillo, J.G.; Lu, C.C.; Cramer, C.J.; Bhan, A.; Gagliardi, L. Influence of First and Second Coordination Environment on Structural Fe(II) Sites in MIL-101 for C–H Bond Activation in Methane. *ACS Catal.* **2021**, *11*, 579–589. [\[CrossRef\]](#)
85. Wang, V.C.-C.; Maji, S.; Chen, P.P.-Y.; Lee, H.K.; Yu, S.S.-F.; Chan, S.I. Alkane Oxidation: Methane Monooxygenases, Related Enzymes, and Their Biomimetics. *Chem. Rev.* **2017**, *117*, 8574–8621. [\[CrossRef\]](#)
86. Bagherzadeh Mostaghimi, A.H.; Al-Attas, T.A.; Kibria, M.G.; Siahrostami, S. A Review on Electrocatalytic Oxidation of Methane to Oxygenates. *J. Mater. Chem. A* **2020**, *8*, 15575–15590. [\[CrossRef\]](#)
87. Latimer, A.A.; Kakekhani, A.; Kulkarni, A.R.; Nørskov, J.K. Direct Methane to Methanol: The Selectivity–Conversion Limit and Design Strategies. *ACS Catal.* **2018**, *8*, 6894–6907. [\[CrossRef\]](#)
88. O'Reilly, M.E.; Kim, R.S.; Oh, S.; Surendranath, Y. Catalytic Methane Monofunctionalization by an Electrogenerated High-Valent Pd Intermediate. *ACS Cent. Sci.* **2017**, *3*, 1174–1179. [\[CrossRef\]](#)
89. Hammond, C.; Forde, M.M.; Ab Rahim, M.H.; Thetford, A.; He, Q.; Jenkins, R.L.; Dimitratos, N.; Lopez-Sanchez, J.A.; Dummer, N.F.; Murphy, D.M.; et al. Direct Catalytic Conversion of Methane to Methanol in an Aqueous Medium by Using Copper-Promoted Fe-ZSM-5. *Angew. Chem. Int. Ed.* **2012**, *51*, 5129–5133. [\[CrossRef\]](#)

90. Antil, N.; Chauhan, M.; Akhtar, N.; Newar, R.; Begum, W.; Malik, J.; Manna, K. Metal–Organic Framework-Encaged Monomeric Cobalt(III) Hydroperoxides Enable Chemoselective Methane Oxidation to Methanol. *ACS Catal.* **2022**, *12*, 11159–11168. [[CrossRef](#)]
91. Tang, X.; Wang, L.; Yang, B.; Fei, C.; Yao, T.; Liu, W.; Lou, Y.; Dai, Q.; Cai, Y.; Cao, X.-M.; et al. Direct Oxidation of Methane to Oxygenates on Supported Single Cu Atom Catalyst. *Appl. Catal. B* **2021**, *285*, 119827. [[CrossRef](#)]
92. Zhao, W.; Shi, Y.; Jiang, Y.; Zhang, X.; Long, C.; An, P.; Zhu, Y.; Shao, S.; Yan, Z.; Li, G.; et al. Fe–O Clusters Anchored on Nodes of Metal–Organic Frameworks for Direct Methane Oxidation. *Angew. Chem. Int. Ed.* **2021**, *60*, 5811–5815. [[CrossRef](#)] [[PubMed](#)]
93. Fang, G.; Hu, J.; Tian, L.; Liang, J.; Lin, J.; Li, L.; Zhu, C.; Wang, X. Zirconium-oxo Nodes of Mofs with Tunable Electronic Properties Provide Effective •OH Species for Enhanced Methane Hydroxylation. *Angew. Chem. Int. Ed.* **2022**, *61*, e202205077. [[CrossRef](#)] [[PubMed](#)]
94. Fang, G.; Wei, F.; Lin, J.; Zhou, Y.; Sun, L.; Shang, X.; Lin, S.; Wang, X. Retrofitting Zr-Oxo Nodes of UiO-66 by Ru Single Atoms to Boost Methane Hydroxylation with Nearly Total Selectivity. *J. Am. Chem. Soc.* **2023**, *145*, 13169–13180. [[CrossRef](#)]
95. Xiao, P.; Wang, Y.; Lu, Y.; De Baerdemaeker, T.; Parvulescu, A.-N.; Müller, U.; De Vos, D.; Meng, X.; Xiao, F.-S.; Zhang, W.; et al. Effects of Al Distribution in the Cu-Exchanged AEI Zeolites on the Reaction Performance of Continuous Direct Conversion of Methane to Methanol. *Appl. Catal. B* **2023**, *325*, 122395. [[CrossRef](#)]
96. Rungtaweeworanit, B.; Abdel-Mageed, A.M.; Khemthong, P.; Eaimsumang, S.; Chakarawet, K.; Butburee, T.; Kunkel, B.; Wohlrab, S.; Chainok, K.; Phanthasri, J.; et al. Structural Evolution of Iron-Loaded Metal–Organic Framework Catalysts for Continuous Gas-Phase Oxidation of Methane to Methanol. *ACS Appl. Mater. Interfaces* **2023**, *15*, 26700–26709. [[CrossRef](#)]
97. Koishybay, A.; Shantz, D.F. Water Is the Oxygen Source for Methanol Produced in Partial Oxidation of Methane in a Flow Reactor over Cu-SSZ-13. *J. Am. Chem. Soc.* **2020**, *142*, 11962–11966. [[CrossRef](#)]
98. Jin, Z.; Wang, L.; Zuidema, E.; Mondal, K.; Zhang, M.; Zhang, J.; Wang, C.; Meng, X.; Yang, H.; Mesters, C.; et al. Hydrophobic Zeolite Modification for in Situ Peroxide Formation in Methane Oxidation to Methanol. *Science* **2020**, *367*, 193–197. [[CrossRef](#)]
99. Li, W.; Li, Z.; Zhang, H.; Liu, P.; Xie, Z.; Song, W.; Liu, B.; Zhao, Z. Efficient Catalysts of Surface Hydrophobic Cu-BTC with Coordinatively Unsaturated Cu(I) Sites for the Direct Oxidation of Methane. *Proc. Natl. Acad. Sci. USA* **2023**, *120*, e2206619120. [[CrossRef](#)]
100. Kye, S.-H.; Park, H.S.; Zhang, R.; Yang, H.J.; Lee, K.H.; Suh, H.; Kim, J.-G.; Kim, M.G.; Hwang, G.S.; Hur, N.H. Partial Oxidation of Methane to Methanol by Isolated Pt Catalyst Supported on a CeO<sub>2</sub> Nanoparticle. *J. Chem. Phys.* **2020**, *152*, 054715. [[CrossRef](#)]
101. Lustemberg, P.G.; Palomino, R.M.; Gutiérrez, R.A.; Grinter, D.C.; Vorokhta, M.; Liu, Z.; Ramírez, P.J.; Matolín, V.; Ganduglia-Pirovano, M.V.; Senanayake, S.D.; et al. Direct Conversion of Methane to Methanol on Ni-Ceria Surfaces: Metal–Support Interactions and Water-Enabled Catalytic Conversion by Site Blocking. *J. Am. Chem. Soc.* **2018**, *140*, 7681–7687. [[CrossRef](#)] [[PubMed](#)]
102. Kwon, Y.; Kim, T.Y.; Kwon, G.; Yi, J.; Lee, H. Selective Activation of Methane on Single-Atom Catalyst of Rhodium Dispersed on Zirconia for Direct Conversion. *J. Am. Chem. Soc.* **2017**, *139*, 17694–17699. [[CrossRef](#)] [[PubMed](#)]
103. Liu, Z.; Huang, E.; Orozco, I.; Liao, W.; Palomino, R.M.; Rui, N.; Duchoň, T.; Nemšák, S.; Grinter, D.C.; Mahapatra, M.; et al. Water-Promoted Interfacial Pathways in Methane Oxidation to Methanol on a CeO<sub>2</sub>–Cu<sub>2</sub>O Catalyst. *Science* **2020**, *368*, 513–517. [[CrossRef](#)] [[PubMed](#)]
104. Huang, E.; Rui, N.; Rosales, R.; Kang, J.; Nemšák, S.; Senanayake, S.D.; Rodriguez, J.A.; Liu, P. Highly Selective Methane to Methanol Conversion on Inverse SnO<sub>2</sub>/Cu<sub>2</sub>O/Cu(111) Catalysts: Unique Properties of SnO<sub>2</sub> Nanostructures and the Inhibition of the Direct Oxidative Combustion of Methane. *ACS Catal.* **2022**, *12*, 11253–11262. [[CrossRef](#)]
105. Huang, E.; Orozco, I.; Ramírez, P.J.; Liu, Z.; Zhang, F.; Mahapatra, M.; Nemšák, S.; Senanayake, S.D.; Rodriguez, J.A.; Liu, P. Selective Methane Oxidation to Methanol on ZnO/Cu<sub>2</sub>O/Cu(111) Catalysts: Multiple Site-Dependent Behaviors. *J. Am. Chem. Soc.* **2021**, *143*, 19018–19032. [[CrossRef](#)]
106. Ross, M.O.; Rosenzweig, A.C. A Tale of Two Methane Monooxygenases. *J. Biol. Inorg. Chem.* **2017**, *22*, 307–319. [[CrossRef](#)]
107. Dinh, K.T.; Sullivan, M.M.; Serna, P.; Meyer, R.J.; Dincă, M.; Román-Leshkov, Y. Viewpoint on the Partial Oxidation of Methane to Methanol Using Cu- and Fe-Exchanged Zeolites. *ACS Catal.* **2018**, *8*, 8306–8313. [[CrossRef](#)]
108. Simons, M.C.; Prinslow, S.D.; Babucci, M.; Hoffman, A.S.; Hong, J.; Vitillo, J.G.; Bare, S.R.; Gates, B.C.; Lu, C.C.; Gagliardi, L.; et al. Beyond Radical Rebound: Methane Oxidation to Methanol Catalyzed by Iron Species in Metal–Organic Framework Nodes. *J. Am. Chem. Soc.* **2021**, *143*, 12165–12174. [[CrossRef](#)] [[PubMed](#)]
109. Sushkevich, V.L.; Palagin, D.; Ranocchiaro, M.; van Bokhoven, J.A. Selective Anaerobic Oxidation of Methane Enables Direct Synthesis of Methanol. *Science* **2017**, *356*, 523–527. [[CrossRef](#)]
110. Kim, M.S.; Park, K.H.; Cho, S.J.; Park, E.D. Partial Oxidation of Methane with Hydrogen Peroxide over Fe-ZSM-5 Catalyst. *Catal. Today* **2021**, *376*, 113–118. [[CrossRef](#)]
111. Lange, J.-P.; Sushkevich, V.L.; Knorpp, A.J.; Van Bokhoven, J.A. Methane-to-Methanol via Chemical Looping: Economic Potential and Guidance for Future Research. *Ind. Eng. Chem. Res.* **2019**, *58*, 8674–8680. [[CrossRef](#)]
112. Tabor, E.; Dedecek, J.; Mlekodaj, K.; Sobalik, Z.; Andrikopoulos, P.C.; Sklenak, S. Dioxygen Dissociation over Man-Made System at Room Temperature to Form the Active α-Oxygen for Methane Oxidation. *Sci. Adv.* **2020**, *6*, eaaz9776. [[CrossRef](#)] [[PubMed](#)]
113. Dedecek, J.; Tabor, E.; Andrikopoulos, P.C.; Sklenak, S. Splitting Dioxygen over Distant Binuclear Transition Metal Cationic Sites in Zeolites. Effect of the Transition Metal Cation. *Int. J. Quantum Chem.* **2021**, *121*, e26611. [[CrossRef](#)]
114. Mlekodaj, K.; Lemishka, M.; Sklenak, S.; Dedecek, J.; Tabor, E. Dioxygen Splitting at Room Temperature over Distant Binuclear Transition Metal Centers in Zeolites for Direct Oxidation of Methane to Methanol. *Chem. Commun.* **2021**, *57*, 3472–3475. [[CrossRef](#)]

115. Tabor, E.; Lemishka, M.; Sobalik, Z.; Mlekodaj, K.; Andrikopoulos, P.C.; Dedecek, J.; Sklenak, S. Low-Temperature Selective Oxidation of Methane over Distant Binuclear Cationic Centers in Zeolites. *Commun. Chem.* **2019**, *2*, 71. [[CrossRef](#)]
116. Jasin Arachchige, L.; Dong, A.; Wang, T.; Li, H.; Zhang, X.L.; Wang, F.; Su, H.; Sun, C. Mechanistic Insights into Direct Methane Oxidation to Methanol on Single-Atom Transition-Metal-Modified Graphyne. *ACS Appl. Nano Mater.* **2021**, *4*, 12006–12016. [[CrossRef](#)]
117. Snyder, B.E.R.; Vanelderen, P.; Schoonheydt, R.A.; Sels, B.F.; Solomon, E.I. Second-Sphere Effects on Methane Hydroxylation in Cu-Zeolites. *J. Am. Chem. Soc.* **2018**, *140*, 9236–9243. [[CrossRef](#)]
118. Snyder, B.E.R.; Bols, M.L.; Rhoda, H.M.; Plessers, D.; Schoonheydt, R.A.; Sels, B.F.; Solomon, E.I. Cage Effects Control the Mechanism of Methane Hydroxylation in Zeolites. *Science* **2021**, *373*, 327–331. [[CrossRef](#)]
119. Wu, L.; Fan, W.; Wang, X.; Lin, H.; Tao, J.; Liu, Y.; Deng, J.; Jing, L.; Dai, H. Methane Oxidation over the Zeolites-Based Catalysts. *Catalysts* **2023**, *13*, 604. [[CrossRef](#)]
120. Tang, Y.; Li, Y.; Fung, V.; Jiang, D.; Huang, W.; Zhang, S.; Iwasawa, Y.; Sakata, T.; Nguyen, L.; Zhang, X.; et al. Single Rhodium Atoms Anchored in Micropores for Efficient Transformation of Methane under Mild Conditions. *Nat. Commun.* **2018**, *9*, 1231. [[CrossRef](#)]
121. Shan, J.; Li, M.; Allard, L.F.; Lee, S.; Flytzani-Stephanopoulos, M. Mild Oxidation of Methane to Methanol or Acetic Acid on Supported Isolated Rhodium Catalysts. *Nature* **2017**, *551*, 605–608. [[CrossRef](#)] [[PubMed](#)]
122. Moteki, T.; Tominaga, N.; Ogura, M. Mechanism Investigation and Product Selectivity Control on CO-Assisted Direct Conversion of Methane into C1 and C2 Oxygenates Catalyzed by Zeolite-Supported Rh. *Appl. Catal. B* **2022**, *300*, 120742. [[CrossRef](#)]
123. Li, H.; Fei, M.; Troiano, J.L.; Ma, L.; Yan, X.; Tieu, P.; Yuan, Y.; Zhang, Y.; Liu, T.; Pan, X.; et al. Selective Methane Oxidation by Heterogenized Iridium Catalysts. *J. Am. Chem. Soc.* **2023**, *145*, 769–773. [[CrossRef](#)] [[PubMed](#)]
124. Wang, W.; Zhou, W.; Tang, Y.; Cao, W.; Docherty, S.R.; Wu, F.; Cheng, K.; Zhang, Q.; Copéret, C.; Wang, Y. Selective Oxidation of Methane to Methanol over Au/H-MOR. *J. Am. Chem. Soc.* **2023**, *145*, 12928–12934. [[CrossRef](#)]
125. Yu, H.; Jiang, J. Accelerating Catalysts Design by Machine Learning. *Sci. Bull.* **2020**, *65*, 1593–1594. [[CrossRef](#)]
126. Ishikawa, A.; Tateyama, Y. A First-Principles Microkinetics for Homogeneous–Heterogeneous Reactions: Application to Oxidative Coupling of Methane Catalyzed by Magnesium Oxide. *ACS Catal.* **2021**, *11*, 2691–2700. [[CrossRef](#)]
127. Adamji, H.; Nandy, A.; Kevlishvili, I.; Román-Leshkov, Y.; Kulik, H.J. Computational Discovery of Stable Metal–Organic Frameworks for Methane-to-Methanol Catalysis. *J. Am. Chem. Soc.* **2023**, *145*, 14365–14378. [[CrossRef](#)]
128. Andrade, L.S.; Lima, H.H.L.B.; Silva, C.T.P.; Amorim, W.L.N.; Poço, J.G.R.; López-Castillo, A.; Kirillova, M.V.; Carvalho, W.A.; Kirillov, A.M.; Mandelli, D. Metal–Organic Frameworks as Catalysts and Biocatalysts for Methane Oxidation: The Current State of the Art. *Coord. Chem. Rev.* **2023**, *481*, 215042. [[CrossRef](#)]
129. Hall, J.N.; Li, M.; Bollini, P. Light Alkane Oxidation over Well-Defined Active Sites in Metal–Organic Framework Materials. *Catal. Sci. Technol.* **2022**, *12*, 418–435. [[CrossRef](#)]
130. Imyen, T.; Znoutine, E.; Suttipat, D.; Iadrat, P.; Kidkhunthod, P.; Bureekaew, S.; Wattanakit, C. Methane Utilization to Methanol by a Hybrid Zeolite@metal–Organic Framework. *ACS Appl. Mater. Interfaces* **2020**, *12*, 23812–23821. [[CrossRef](#)]
131. Li, S.; Ahmed, R.; Yi, Y.; Bogaerts, A. Methane to Methanol through Heterogeneous Catalysis and Plasma Catalysis. *Catalysts* **2021**, *11*, 590. [[CrossRef](#)]
132. Sher Shah, M.S.A.; Oh, C.; Park, H.; Hwang, Y.J.; Ma, M.; Park, J.H. Catalytic Oxidation of Methane to Oxygenated Products: Recent Advancements and Prospects for Electrocatalytic and Photocatalytic Conversion at Low Temperatures. *Adv. Sci.* **2020**, *7*, 2001946. [[CrossRef](#)] [[PubMed](#)]
133. Lee, J.; Yang, J.; Moon, J.H. Solar Cell-Powered Electrochemical Methane-to-Methanol Conversion with CuO/CeO<sub>2</sub> Catalysts. *ACS Energy Lett.* **2021**, *6*, 893–899. [[CrossRef](#)]
134. Chawdhury, P.; Wang, Y.; Ray, D.; Mathieu, S.; Wang, N.; Harding, J.; Bin, F.; Tu, X.; Subrahmanyam, C. A Promising Plasma-Catalytic Approach towards Single-Step Methane Conversion to Oxygenates at Room Temperature. *Appl. Catal. B* **2021**, *284*, 119735. [[CrossRef](#)]
135. Zhu, S.; Li, X.; Pan, Z.; Jiao, X.; Zheng, K.; Li, L.; Shao, W.; Zu, X.; Hu, J.; Zhu, J.; et al. Efficient Photooxidation of Methane to Liquid Oxygenates over ZnO Nanosheets at Atmospheric Pressure and Near Room Temperature. *Nano Lett.* **2021**, *21*, 4122–4128. [[CrossRef](#)]

**Disclaimer/Publisher’s Note:** The statements, opinions and data contained in all publications are solely those of the individual author(s) and contributor(s) and not of MDPI and/or the editor(s). MDPI and/or the editor(s) disclaim responsibility for any injury to people or property resulting from any ideas, methods, instructions or products referred to in the content.